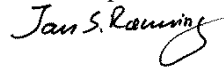


# GEOLOGI FOR SAMFUNNET

*GEOLOGY FOR SOCIETY*





Report no.: 2013.029		ISSN 0800-3416	Grading: Open	
<b>Title:</b> Helicopter-borne magnetic, electromagnetic and radiometric geophysical surveys in the Kongsberg region: Krøderen, Sokna, Hønefoss, Kongsberg and Numedalen.				
<b>Authors:</b> Vikas Baranwal, Alexei Rodionov, Frode Ofstad, Janusz Koziel & Rolf Lynum		<b>Client:</b> NGU / Buskerud-Telemark-Vestfold County cooperation.		
<b>County:</b> Buskerud, Telemark and Vestfold		<b>Municipalities:</b> Andebu, Hof, Hole, Holmestrand, Kongsberg, Krødsherad, Lardal, Modum, Ringerike, Sigdal, Skien, Siljan, Våle og Øvre Eiker		
<b>Map-sheet name (M=1:250.000)</b> Skien and Oslo		<b>Map-sheet no. and -name (M=1:50.000)</b> 1713 I Siljan, 1713 IV Nordagutu, 1714 I Hokksund, 1714 II Kongsberg, 1714 III Notodden, 1714 IV Flesberg 1715 II Krøderen, 1715 III Eggedal, 1815 II Oppkuven 1815 III Hønefoss,		
<b>Deposit name and grid-reference:</b> Kongsberg UTM 32N 545000 - 6627000		<b>Number of pages:</b> 53		<b>Price (NOK):</b> 250,-
<b>Fieldwork carried out:</b> 2008-2011		<b>Date of report:</b> July 2013		<b>Project no.:</b> 327600
				<b>Person responsible:</b> 
<b>Summary:</b> <p>NGU conducted an airborne geophysical survey around Kongsberg region covering Krøderen, Sokna, Hønefoss, Kongsberg, Vikersund, Hokksund and Hvittingfoss regions during 2008-2011. This report describes and documents the acquisition, processing and visualization of recorded datasets. The geophysical survey performed herein results in total 13985 line km that covers approximately an area of 2797 km<sup>2</sup>.</p> <p>A Hummingbird electromagnetic frequency domain system from Geotech Ltd., modified by NGU and an optically pumped Cesium magnetometer were used for electromagnetic (EM) and Magnetic data acquisition. In the first part of the survey, a 256 channel Exploranium GR 820 gamma-ray spectrometer were used while a 1024 channels Radiation Solution's RSX-5 were used in the last part for radiometric data acquisition.</p> <p>The survey was flown with 200 m line spacing, mostly E-W direction with an average speed of 108 km/h. The average terrain clearance of the helicopter was approximately 75 m. Collected data were processed at NGU using Geosoft Oasis Montaj and in-house software. Raw total magnetic field data were corrected for diurnal variation and also for IGRF.</p> <p>Magnetic data are presented as total field anomaly, first order vertical derivative and tilt derivative. EM data were filtered and levelled using both automated and manual levelling procedure. Apparent resistivity was calculated for each frequency from in-phase and quadrature data for three higher frequencies (6606, 7001 and 34133 Hz) however from quadrature only for two lower frequencies (880 and 980 Hz) using a homogeneous half-space model. Radiometric data were processed using standard procedures recommended by International Atomic Energy Association (IAEA) and ground concentration of potassium, equivalent uranium, equivalent thorium were calculated.</p> <p>All data were gridded with the cell size of 50 x 50 m and presented as contour maps at various scales.</p>				
<b>Keywords:</b> Geophysics		Airborne		Magnetic
Electromagnetic		Gamma spectrometry		Radiometric
				Technical report





## Table of Contents

1. INTRODUCTION.....	7
2. LOCATION.....	7
3. SURVEY SPECIFICATIONS .....	9
3.1 Airborne Survey Parameters.....	9
3.2 Airborne Survey Instrumentation .....	10
3.3 Airborne Survey Logistics Summary .....	11
3.4 Calibrations.....	11
4. DATA PROCESSING AND PRESENTATION .....	12
4.1 Total Magnetic Field Data .....	12
4.2 Electromagnetic Data .....	13
4.3 Radiometric data .....	14
5. PRODUCTS.....	14
6. REFERENCES.....	16
Appendix A: Short description of magnetic, electromagnetic and radiometry methods	48
Appendix B1: Flow chart of magnetic processing.....	51
Appendix B2: Flow chart of EM processing.....	51
Appendix B3: Flow chart of radiometry processing.....	51
Appendix C: Description of channel labels used in XYZ files .....	53

## FIGURES

Figure 1: Survey areas around Kongsberg region in Telemark, Buskerud and Vestfold counties. See text for details. ....	8
Figure 2: Hummingbird system in the air during a survey.....	11
Figure 3: Total magnetic field anomaly map of Kongsberg-I area. ....	18
Figure 4: First vertical derivative magnetic map of Kongsberg-I area. ....	18
Figure 5: Tilt derivative magnetic map of Kongsberg-I area. ....	19
Figure 6: Total magnetic field anomaly map of Kongsberg-II area.....	19
Figure 7: First vertical derivative magnetic map of Kongsberg-II area.....	20
Figure 8: Tilt derivative magnetic map of Kongsberg-II area.....	21
Figure 9: Total magnetic field anomaly map of Kongsberg-III area. ....	22
Figure 10: First vertical derivative magnetic map of Kongsberg-III area. ....	23
Figure 11: Tilt derivative magnetic map of Kongsberg-III area. ....	24
Figure 12: Total radiation count map of Kongsberg-I area.....	25
Figure 13: Ground concentration map of potassium from Kongsberg-I.....	25
Figure 14: Ground concentration map of equivalent uranium from Kongsberg-I.....	26
Figure 15: Ground concentration map of equivalent thorium from Kongsberg-I. ....	26
Figure 16: Ternary radiation map from Kongsberg-I.....	27

<b>Figure 17: Total radiation count map from Kongsberg-II.....</b>	<b>27</b>
<b>Figure 18: Ground concentration map of potassium from Kongsberg-II. ....</b>	<b>28</b>
<b>Figure 19: Ground concentration map of equivalent uranium from Kongsberg-II.....</b>	<b>29</b>
<b>Figure 20: Ground concentration map of equivalent thorium from Kongsberg-II.....</b>	<b>30</b>
<b>Figure 21: Ternary radiation map from Kongsberg-II. ....</b>	<b>31</b>
<b>Figure 22: Total radiation count map from Kongsberg-III. ....</b>	<b>32</b>
<b>Figure 23: Ground concentration map of potassium from Kongsberg-III.....</b>	<b>33</b>
<b>Figure 24: Ground concentration map of equivalent uranium from Kongsberg-III. ....</b>	<b>34</b>
<b>Figure 25: Ground concentration map of equivalent thorium from Kongsberg-III. ....</b>	<b>35</b>
<b>Figure 26: Ternary radiation map from Kongsberg-I.....</b>	<b>36</b>
<b>Figure 27: Apparent resistivity map from frequency 880 Hz from Kongsberg-I. ....</b>	<b>37</b>
<b>Figure 28: Apparent resistivity map from frequency 980 Hz from Kongsberg-I. ....</b>	<b>37</b>
<b>Figure 29: Apparent resistivity map from frequency 6606 Hz from Kongsberg-I. ....</b>	<b>38</b>
<b>Figure 30: Apparent resistivity map from frequency 7001 Hz from Kongsberg-I. ....</b>	<b>38</b>
<b>Figure 31: Apparent resistivity map from frequency 34133 Hz from Kongsberg-I. ....</b>	<b>39</b>
<b>Figure 32: Apparent resistivity map from frequency 980 Hz from Kongsberg-II.....</b>	<b>39</b>
<b>Figure 33: Apparent resistivity map from frequency 6606 Hz from Kongsberg-II.....</b>	<b>40</b>
<b>Figure 34: Apparent resistivity map from frequency 7001 Hz from Kongsberg-II.....</b>	<b>41</b>
<b>Figure 35: Apparent resistivity map from frequency 34133 Hz from Kongsberg-II.....</b>	<b>42</b>
<b>Figure 36: Apparent resistivity map from frequency 880 Hz from Kongsberg-III. ....</b>	<b>43</b>
<b>Figure 37: Apparent resistivity map from frequency 980 Hz from Kongsberg-I. ....</b>	<b>44</b>
<b>Figure 38: Apparent resistivity map from frequency 6606 Hz from Kongsberg-III.....</b>	<b>45</b>
<b>Figure 39: Apparent resistivity map from frequency 7001 Hz from Kongsberg-III. ....</b>	<b>46</b>
<b>Figure 40: Apparent resistivity map from frequency 34133 Hz from Kongsberg-III. ....</b>	<b>47</b>

**TABLES**

<b>Table 1. Instrument Specifications .....</b>	<b>10</b>
<b>Table 2. Frequencies and coil configurations of Hummingbird electromagnetic system</b>	<b>10</b>
<b>Table 3: Maps in scale 1:50000, 1:100000 and 1:120000 available from NGU on request</b>	<b>15</b>

## **1. INTRODUCTION**

The objective of the airborne geophysical survey was to obtain a dense high-resolution aeromagnetic, electromagnetic and radiometric data over the survey area. This data is required for the enhancement of a general understanding of the regional geology of the area. In this regard, the data can also be used to map contacts and structural features. It also improves defining the potential of known zones of mineralization, their geological settings, and identifying new areas of interest. Acquired data will also be used for location of possible tunnel construction problems, evaluation of possible radon problems in houses and characterisation of soft sediments.

The survey incorporated the use of a Hummingbird™ five-frequency electromagnetic (EM) system supplemented by a high-sensitivity caesium magnetometer, gamma-ray spectrometer and radar altimeter. A GPS navigation computer system with flight path indicators ensured accurate positioning of the geophysical data with respect to the World Geodetic System 1984 Geodetic datum (WGS-84).

## **2. LOCATION**

The survey area is situated in west of Oslofjord in Telemark (small area), Buskerud and Vestfold counties, Norway (see figure 1). Survey area is marked with three polygons in red, black and blue colours representing Kongsberg-I, Kongsberg-II and Kongsberg-III, respectively. Kongsberg-I including Krøderen, Sokna and Honefoss was surveyed in autumn of 2010. Kongsberg-II, covering areas around Vikersund, Hokksund and Kongsberg, was surveyed in autumn of 2008 and summer of 2009 and finally Kongsberg-III containing areas around Numedalen valley and Hvittingfoss was surveyed in May and July of 2011.



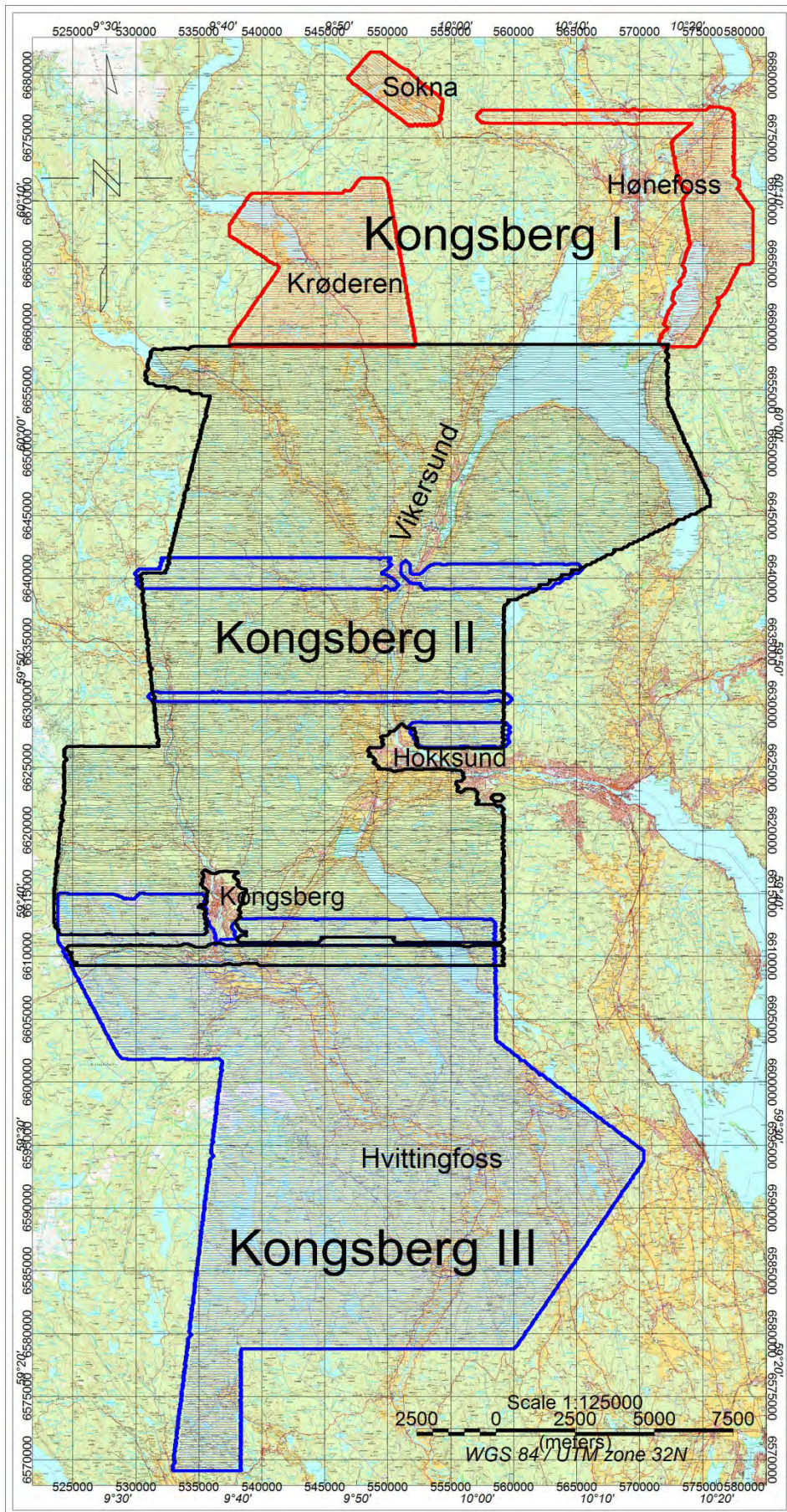


Figure 1: Survey areas around Kongsberg region in Telemark, Buskerud and Vestfold counties. See text for details.

### 3. SURVEY SPECIFICATIONS

Airborne magnetic, EM and gamma-ray spectrometry data were measured in the survey area. A brief description of these methods is discussed in Appendix A.

#### 3.1 Airborne Survey Parameters

NGU used a Hummingbird™ EM and magnetic helicopter survey system designed to obtain low level, slow speed, detailed airborne magnetic and EM data (Geotech 1997). In addition, a 256 channel Exploranium GR820 gamma-ray spectrometer initially and a 1024 channel Radiation Solutions RSX-5 gamma-ray spectrometer later in the survey were used to map ground concentrations of uranium (U), thorium (Th) and potassium (K) .

The airborne survey began in autumn 2008 and was carried out in different parts of area till summer 2011. For all flights, a Eurocopter AS350-B2 helicopter was used to tow the bird. Helicopters were operated by Pegasus As. (2008-2009), Airlift As. (2010) and Heliscan (2011). The flight lines were spaced 200 m apart in UTM zone 32N coordinates and in E-W direction in most of the survey except a small area in Sokna of Kongsberg-I which was oriented around 140° azimuth. The line directions were selected according to geological strike in the area.

The magnetic and EM sensors were housed in a single 7.5 m long bird, which was maintained at an average of around 45 m above the topographic surface. Gamma-rays spectrometer installed under the belly of the helicopter registered natural gamma ray radiation at an average height of 75 m from the ground simultaneously with the acquisition of magnetic and EM data.

In airborne radiometry surveys, it is assumed that footprint of the measurements is an oval of width twice the flying height, and length twice the flying height and the distance travelled during the measurement, i.e. roughly 120 m and 150 m, respectively for a sensor height of 60 m and a speed of 100 km/h. Rugged terrain and abrupt changes in topography may affect the pilot's ability to 'drape' the terrain, therefore there were variations in sensor height with respect to the estimated range, which was higher than the standard heights of 35 m (for magnetic and EM survey) and 65 m ( for radiometry survey).

The ground speed of the aircraft varied from 50 to 120 km/h depending on the topography, wind direction and its speed. On average the ground speed during measurements was calculated to 108 km/h. Magnetic data were recorded at 0.2 second intervals resulting in approximately 6 m point spacing. EM data were recorded at 0.1 second intervals resulting in data with an average sample increment of 3 m. Spectrometry data were recorded every 1 second giving a point spacing of approximately 30 meter. The above parameters were designed to allow for sufficient details in the data to detect subtle anomalies that might represent mineralization and/or rocks of different lithological and petrophysical composition.

A base magnetometer to monitor diurnal variations in the magnetic field was located at various suitable places generally, close to the airports, within the 20 km of the survey areas. Base station magnetometer data were recorded once every 3 second. The CPU clock of the base magnetometer computer was synchronized to the CPU clock of the Digital Acquisition System (DAS) on a daily basis.



Navigation system used GPS/GLONASS satellite tracking systems to provide real-time WGS-84 coordinate locations for every second. The accuracy achieved without differential corrections was reported to be  $\pm 5$  m in the horizontal directions. The GPS receiver antenna was mounted externally to the tail tip of the helicopter.

### 3.2 Airborne Survey Instrumentation

The instrument specifications are given in table 1. Frequencies and coil configuration for the Hummingbird EM system is given in table 2.

**Table 1. Instrument Specifications**

<b>Instrument</b>	<b>Producer/Model</b>	<b>Accuracy</b>	<b>Sampling frequency</b>
Magnetometer	Scintrex Cs-2	0,002 nT	5 Hz
Base magnetometer	Scintrex EnviMag	0,1 nT	0,33 Hz
Electromagnetic	Geotech Hummingbird	1 – 2 ppm	10 Hz
Gamma ray-spectrometer	Exploranium GR 820 Radiation Solutions RSX-5	256/1024 channels, 16 liters down, 4 liters up	1 Hz
Radar altimeter	Bendix/King KRA 405B	$\pm 3\%$ 0 – 500 fot $\pm 5\%$ 500 – 2500 fot	1 Hz
Pressure/temperature	Honeywell PPT	$\pm 0,03\%$ FS	1 Hz
Navigation	Topcon GPS-receiver	$\pm 5$ meter	1 Hz
Acquisition system	Geotech Ltd and NGU In-house software		

**Table 2. Frequencies and coil configurations of Hummingbird electromagnetic system**

<b>Coils:</b>	<b>Frequency</b>	<b>Orientation</b>	<b>Separation</b>
A	7701 Hz	Coaxial	6.2 m
B	6606 Hz	Coplanar	6.2 m
C	980 Hz	Coaxial	6.0 m
D	880 Hz	Coplanar	6.0 m
E	34133 Hz	Coplanar	4.9 m

The EM, magnetic, radiometric, altitude and navigation data were monitored on the operator's display during the flight for quality control and survey progress. The collected survey data were also stored to the PC/external hard disk drive. Spectrometry data were also recorded to internal hard drive of the spectrometer. The raw data files were backed up onto USB flash drive in the field.

### 3.3 Airborne Survey Logistics Summary

Traverse (survey) line spacing:	200 metres
Traverse line direction:	E-W (except 140° azimuth for Sokna)
Nominal aircraft ground speed:	30 - 120 km/h
Average sensor terrain clearance EM+Mag:	45 metres
Average sensor terrain clearance Rad:	75 metres
Sampling rates:	0.2 seconds - magnetometer 0.1 seconds - electromagnetic 1.0 second - spectrometer, GPS and radar altimeter

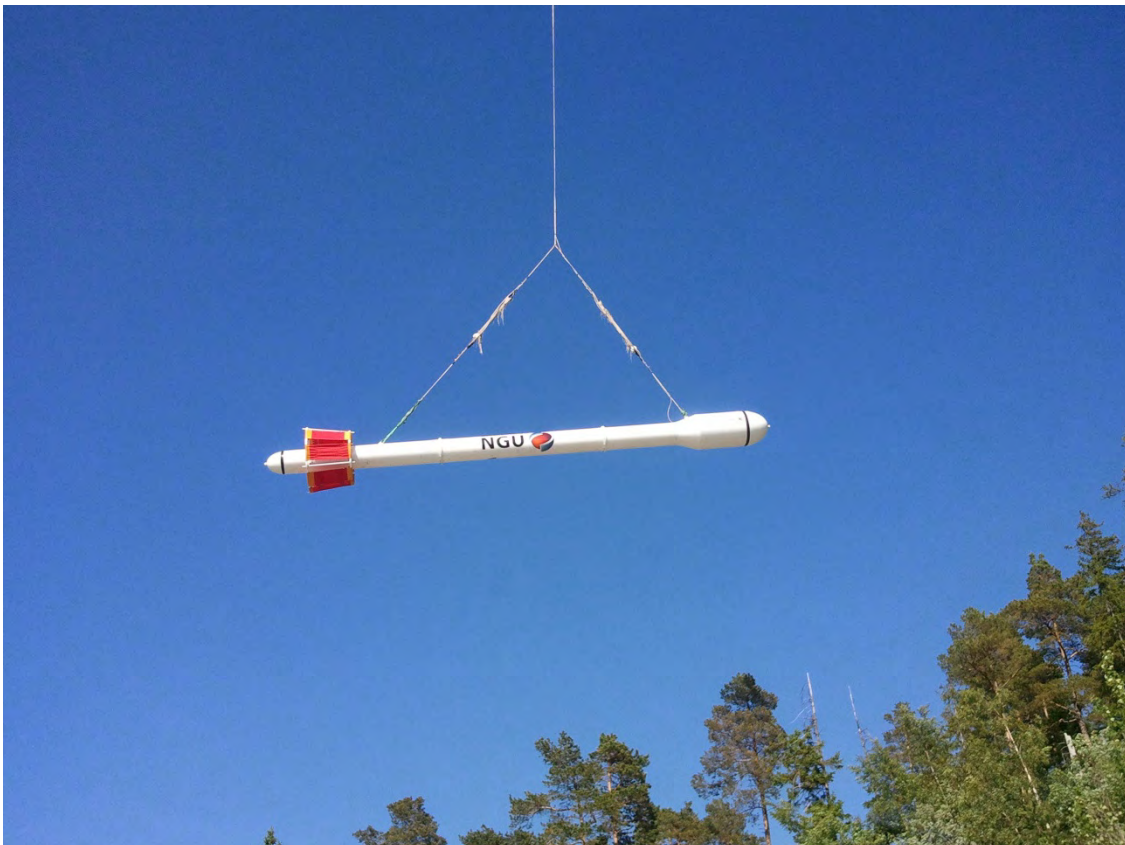


Figure 2: Hummingbird system in the air during a survey

### 3.4 Calibrations

Gamma-ray spectrometers were calibrated for K, U and Th sensitivity over mobile pads at NGU annually before starting of the surveys. Stripping ratios and sensitivities for K, U and Th were also calculated in Borlange, Sweden over special K, U, Th pads (fixed installation for radiometric calibration purpose) in June 2012 (Grasty et al., 1991, Appendix A). Cosmic coefficients and aircraft background were determined from a special survey as recommended by IAEA (2003). Height attenuation coefficients were calculated from a special survey in Kviteseid area following the recommendations of IAEA (2003). Upward detectors were used to correct for atmospheric radon measurements.

EM system was calibrated for phasing with the help of ferrite bar and for resistivity calculation using calibration coils as recommended by manufacturers (Geotech, 1997).

## 4. DATA PROCESSING AND PRESENTATION

All the survey data were processed at the Geological Survey of Norway office in Trondheim. The ASCII data files were loaded into three separate Oasis Montaj databases. All three datasets were processed consequently according to the processing flow charts shown in Appendices B1, B2 and B3.

### 4.1 Total Magnetic Field Data

At the first stage the total magnetic field data were visually inspected and spikes were removed manually. Then the data from basemag station were imported in magnetic database using the standard Oasis magbase.gx module. Basemag channel was also inspected for spikes and spikes were removed manually if necessary. Since the data from both airborne and base magnetometers were smooth and contained no significant cultural noise, filtering of the raw data was not necessary. The temporal fluctuations in the magnetic field of the earth affect the total magnetic field readings recorded during the airborne survey. This is commonly referred to as the magnetic diurnal variation. These fluctuations can be effectively removed from the airborne magnetic data set by using a stationary reference magnetometer that records the magnetic field of the earth simultaneously with the airborne sensor. Magnetic diurnals were within the standard NGU specifications during the entire survey (Rønning, 2013).

The base magnetometer was located at the various places generally, close to the airports, within 20 km of the survey area. The average total magnetic field value for base stations were 51012, 50502 and 50134 nT for Kongsberg-I, Kongsberg-II and Kongsberg-III, respectively. The base station computer clock was synchronized with the DAS clock on a daily basis. International geomagnetic reference field (IGRF) for 2010 was calculated for each measurement points of the survey area using Geosoft gx 'IGRF' and subtracted from the measured magnetic field to obtain total magnetic field anomaly as shown in eq. 1.

$$\mathbf{B}_{Ta} = \mathbf{B}_T + (\bar{\mathbf{B}}_B - \mathbf{B}_B) - \mathbf{B}_{IGRF} \quad (1)$$

where  $\mathbf{B}_{Ta}$  is total magnetic field anomaly,  $\mathbf{B}_T$  is total magnetic field measured from helicopter,  $\mathbf{B}_B$  is base magnetometer reading,  $\bar{\mathbf{B}}_B$  is average of base magnetometer reading and  $\mathbf{B}_{IGRF}$  is IGRF value for measurement points in the survey area.

Lag between logged magnetic data and the corresponding navigational data was 1 to 2 fiducial. Translated to a distance it would be no more than 8 m - the value comparable with the precision of the GPS. Therefore a heading error for a towed system is usually either very small or non-existent. So no lag and heading corrections were applied. A flow chart of the magnetic data processing (including the used parameters) is given in Appendix B1. An overview of standard processing for airborne magnetic data is given by e.g. Minty et al. (1997). Flight data were split in flight lines before gridding. For the purposes of data presentation and interpretation, the total magnetic field anomaly data were gridded using minimum curvature method with a cell size of 50 m, which represents one quarter of the average line spacing of 200 m.

1<sup>st</sup> vertical derivative and tilt-derivative of the total magnetic field anomaly were calculated from the resulting total magnetic field anomaly grid using appropriate convolution filters available in Geosoft Oasis Montaj. 1<sup>st</sup> vertical derivative shows the change of magnetic field anomaly with vertical distance close to the surface. Tilt derivative is arctangent of vertical and total horizontal derivatives and it is useful to enhance lineaments/trends. Both 1<sup>st</sup> vertical derivative and tilt derivative will concentrate magnetic anomaly just above the magnetic body.

## 4.2 Electromagnetic Data

The DAS computer records both an in-phase and a quadrature value for each of the five coil sets of the electromagnetic system. Instrumental noise and drift should be removed before computation of an apparent resistivity. No data were collected for 880 Hz during the survey of Kongsberg-II area because of an instrument failure.

In-phase and quadrature data were filtered with 3 fiducials non-linear filter to eliminate spheric spikes which were represented as irregular spikes of large amplitude in records. Simultaneously, the 20 fiducials low-pass filter was also applied to suppress high frequency components of instrumental and cultural noise.

In order to remove the effects of instrument drift caused by gradual temperature variations in the transmitting and receiving circuits, background responses were recorded during each flight. To obtain a background level, the bird was raised to an altitude of approximately 1200 ft above the topographic surface so that no electromagnetic responses from the ground were present in the recorded traces. The EM traces observed at this altitude correspond to a background (zero) level of the system. If these background levels were recorded at 20-30 minute intervals, then the drift of the system (assumed to be linear) could be removed from the data by resetting these points to the initial zero level of the system (Valleau, 2000). The drift was removed on a flight-by-flight basis before any further processing was carried out. Geosoft HEM module was used for applying drift correction. Residual instrumental drift, often non-linear, was manually removed on line-to-line basis. The EM data was not very smooth and it had several non-linear variations due to various instrumental errors and instability problems. However maximum efforts were made to bring the data at a level so that the instrumental drift was removed and no artificial level was introduced in the data.

After levelling of the HEM data, apparent resistivity was calculated from in-phase and quadrature EM components using a half space homogeneous model of the Earth (Geosoft HEM module) for all five frequencies separately. Threshold of 3 ppm was set for inversion of three higher frequencies of 6606, 7001 and 34133 kHz and 2 ppm for lower frequencies of 880 and 980 Hz. However it was observed that resistivity map obtained using inversion of both in-phase and quadrature data for lower frequencies were not consistent.

Secondary electromagnetic field decays rapidly with the distance  $z$  (height of the sensors from the target) as  $1/z^2$  to  $1/z^5$  depending on the shape of the conductors and, at certain height, signals from the ground sources become comparable with instrumental noise. Levelling errors or precision of levelling can lead sometimes to appearance of artificial resistivity anomalies when data were collected at high instrumental altitude. Application of threshold allows excluding such data from an apparent resistivity calculation, though not completely. It's particularly noticeable in low frequencies datasets. Therefore, resistivity data were visually inspected for artificial anomalies associated with high altitude measurements. They were

manually removed and then re-levelled. Finally, revised resistivity data were gridded with a cell size of 50 m.

Temperature drift of the EM-frequencies were partly above standard NGU specifications during the 2008-2011 survey (Rønning 2013). Therefore resulted EM resistivity grids were not as good as it was supposed to be. EM data at lower frequencies had lesser amplitude compared to higher frequencies. When data was not of good quality then apparent resistivity calculated from In-phase (which was a response from both magnetic and conductive bodies) and quadrature (which was a response only by conductive bodies) could be inconsistent and erroneous. Therefore apparent resistivity calculated from quadrature components only were presented for 880 and 980 Hz frequencies.

### **4.3 Radiometric data**

In processing of the airborne gamma ray spectrometry data, live time corrected Total count (TC), equivalent Uranium (eU), equivalent Thorium (eTh) and Potassium (K) window data were corrected for the aircraft and cosmic background (e.g. Minty et al. 1997; IAEA 2003). The upward detector method, as discussed in IAEA (2003), was applied to remove the effects of radon in the air below and around the helicopter. Window stripping was used to isolate count rates from the individual radio-nuclides K, eU and eTh (IAEA, 2003). The topography in the region was rough, and the sensor was not always at a constant altitude. Stripped window counts were therefore corrected for variations in flying height to a constant height of 60 m. Finally, count rates were converted to effective ground element concentrations using calibration values derived from NGU mobile pads. A list of the parameters used in the processing scheme is given in Appendix B2. For further reading regarding standard processing of airborne radiometric data, we recommend the publication from Minty et al. (1997) and IAEA, 2003.

Flight data were split in flight lines before gridding. Final TC, K, eU and eTh data were gridded with a cell size of 50 m. A micro-leveling technique was applied to them to remove small, along the line leveling errors when required.

## **5. PRODUCTS**

Processed digital data from the survey were presented as:

1. Nine Geosoft XYZ files containing three files for magnetic, EM and radiometry, respectively for each of the three areas Kongsberg-I, Kongsberg-II and Kongsberg-III as Kongsberg\_MAG\_Area1.XYZ, Kongsberg\_EM\_Area1, Kongsberg\_RAD\_Area1.XYZ, Kongsberg\_MAG\_Area2.XYZ, Kongsberg\_EM\_Area2, Kongsberg\_RAD\_Area2.XYZ, Kongsberg\_MAG\_Area3.XYZ, Kongsberg\_EM\_Area3, Kongsberg\_RAD\_Area3.XYZ
2. Coloured maps at the scales 1:50000, 1:100000 and 1:120000 for Kongsberg-I, Kongsberg-II and Kongsberg-III, respectively are available from NGU on request.

Table 3 describes various available maps with reference number. Downscaled images of all the maps are shown in figure 3-40. A brief description of channel labels used in XYZ files are explained in Appendix-C.



**Table 3: Maps in scale 1:50000, 1:100000 and 1:120000 available from NGU on request**

Map #	Name
2013.029-01	Total magnetic field anomaly from Kongsberg-I
2013.029-02	Magnetic Vertical Derivative from Kongsberg-I
2013.029-03	Magnetic Tilt Derivative from Kongsberg-I
2013.029-04	Total magnetic field anomaly from Kongsberg-II
2013.029-05	Magnetic Vertical Derivative from Kongsberg-II
2013.029-06	Magnetic Tilt Derivative from Kongsberg-II
2013.029-07	Total magnetic field anomaly from Kongsberg-III
2013.029-08	Magnetic Vertical Derivative from Kongsberg-III
2013.029-09	Magnetic Tilt Derivative from Kongsberg-III
2013.027-10	Total radiation count from Kongsberg-I
2013.027-11	Potassium ground concentration from Kongsberg-I
2013.027-12	Equivalent uranium ground concentration from Kongsberg-I
2013.027-13	Equivalent thorium ground concentration from Kongsberg-I
2013.027-14	Radiometric Ternary Map from Kongsberg-I
2013.027-15	Total radiation count from Kongsberg-II
2013.027-16	Potassium ground concentration from Kongsberg-II
2013.027-17	Equivalent uranium ground concentration from Kongsberg-II
2013.027-18	Equivalent thorium ground concentration from Kongsberg-II
2013.027-19	Radiometric Ternary Map from Kongsberg-II
2013.027-20	Total radiation count from Kongsberg-III
2013.027-21	Potassium ground concentration from Kongsberg-III
2013.027-22	Equivalent uranium ground concentration from Kongsberg-III
2013.027-23	Equivalent thorium ground concentration from Kongsberg-III
2013.027-24	Radiometric Ternary Map from Kongsberg-III
2013.027-25	Apparent resistivity at frequency 880 Hz from Kongsberg-I
2013.027-26	Apparent resistivity at frequency 980 Hz from Kongsberg-I
2013.027-27	Apparent resistivity at frequency 6606 Hz from Kongsberg-I
2013.027-28	Apparent resistivity at frequency 7001 Hz from Kongsberg-I
2013.027-29	Apparent resistivity at frequency 34133 Hz from Kongsberg-I
2013.027-30	Apparent resistivity at frequency 980 Hz from Kongsberg-II
2013.027-31	Apparent resistivity at frequency 6606 Hz from Kongsberg-II
2013.027-32	Apparent resistivity at frequency 7001 Hz from Kongsberg-II
2013.027-33	Apparent resistivity at frequency 34133 Hz from Kongsberg-II
2013.027-34	Apparent resistivity at frequency 880 Hz from Kongsberg-III
2013.027-35	Apparent resistivity at frequency 980 Hz from Kongsberg-III
2013.027-36	Apparent resistivity at frequency 6606 Hz from Kongsberg-III
2013.027-37	Apparent resistivity at frequency 7001 Hz from Kongsberg-III
2013.027-38	Apparent resistivity at frequency 34133 Hz from Kongsberg-III

A compilation of all these data together with other data from the neighbouring areas will be published separately.

## 6. REFERENCES

Geotech 1997: Hummingbird Electromagnetic System. User's manual. Geotech Ltd. October 1997.

Grasty, R.L., Holman, P. B. & Blanchard 1991: Transportable Calibration pads for ground and airborne Gamma-ray Spectrometers. Geological Survey of Canada. Paper 90-23. 62 pp.

IAEA 2003: Guidelines for radioelement mapping using gamma ray spectrometry data. IAEA-TECDOC-1363, Vienna, Austria. 173 pp.

Minty, B.R.S., Luyendyk, A.P.J. and Brodie, R.C. 1997: Calibration and data processing for gamma-ray spectrometry. AGSO – Journal of Australian Geology & Geophysics. 17(2). 51-62.

Oasis Montaj Geosoft. 2007. Quick start tutorial – Mapping and processing system. (PDF-download of tutorial is available on webpage: <http://www.geosoft.com/resources/tutorials/>).

Rønning, J.S., Kihle, O., Mogaard, J.O., Walker, P., Shomali, H., Hagthorpe, P., Byström, S., Lindberg, H. and Thunehed, H. 2003. Forsmark site investigation – Helicopter borne geophysics at Forsmark, Ôsthammar, Sweden. *SKB report P-03-41*. 137 pp.

Rønning, J.S. 2013: NGUs helikoptermålinger. Plan for sikring og kontroll av datakvalitet. Versjon 4, NGU Intern rapport 2013.001, pp. 38.

Valleau, N.C. 2000. HEM data processing - a practical overview. *Exploration Geophysics*, 31, 584-594.



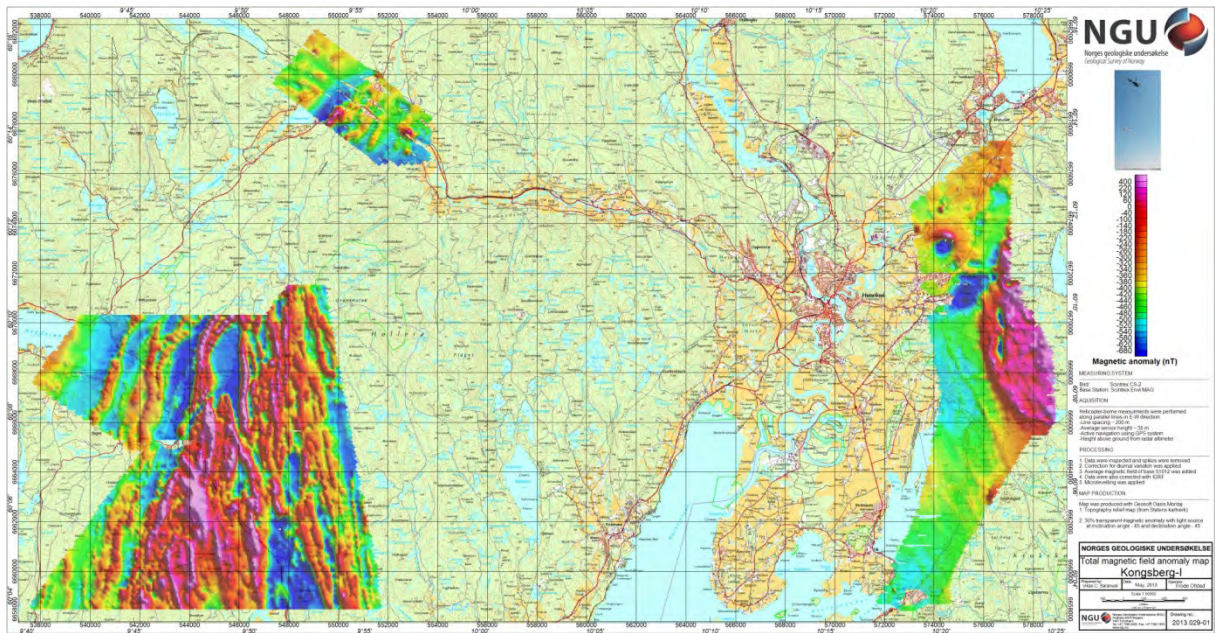


Figure 3: Total magnetic field anomaly map of Kongsberg-I area.

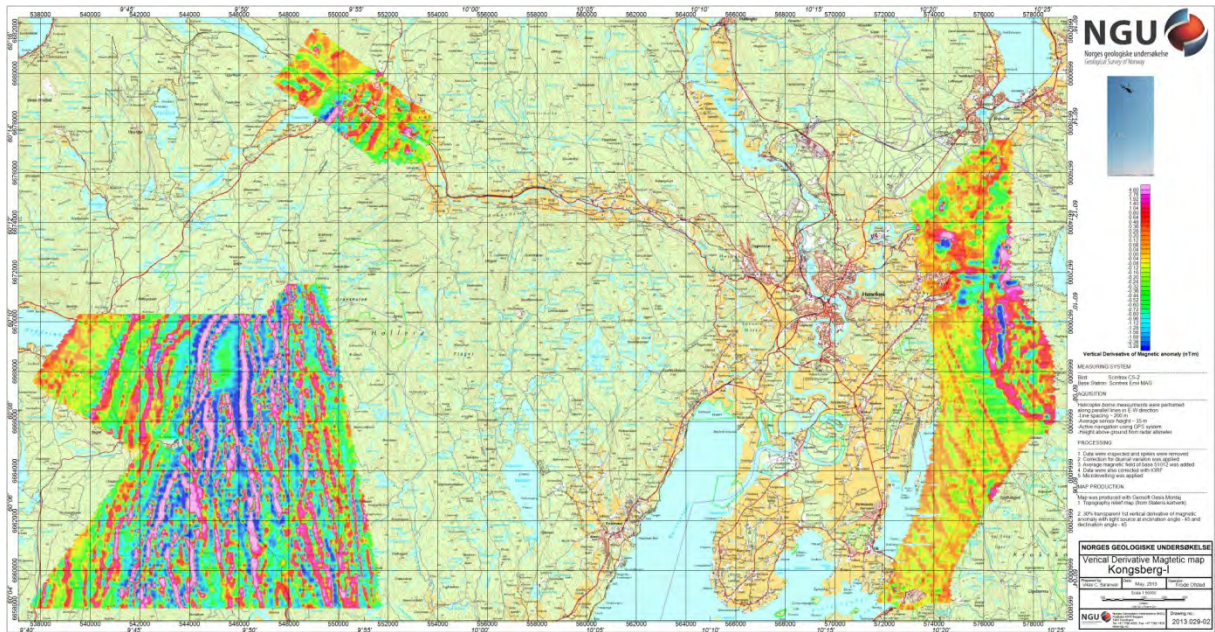


Figure 4: First vertical derivative magnetic map of Kongsberg-I area.



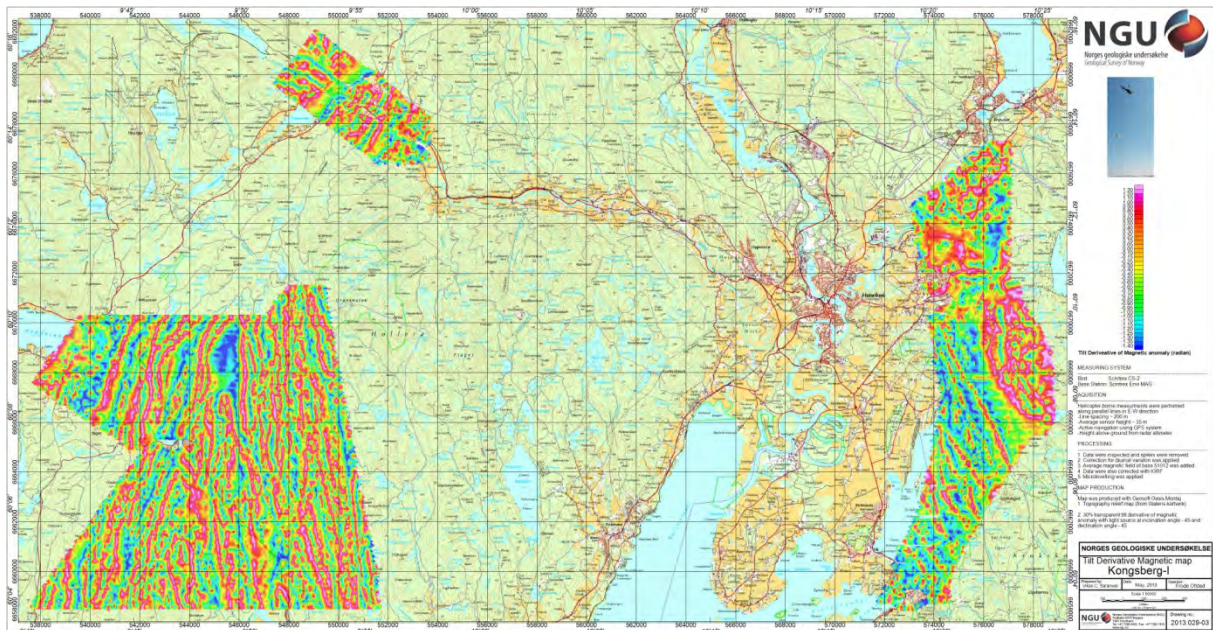


Figure 5: Tilt derivative magnetic map of Kongsberg-I area.

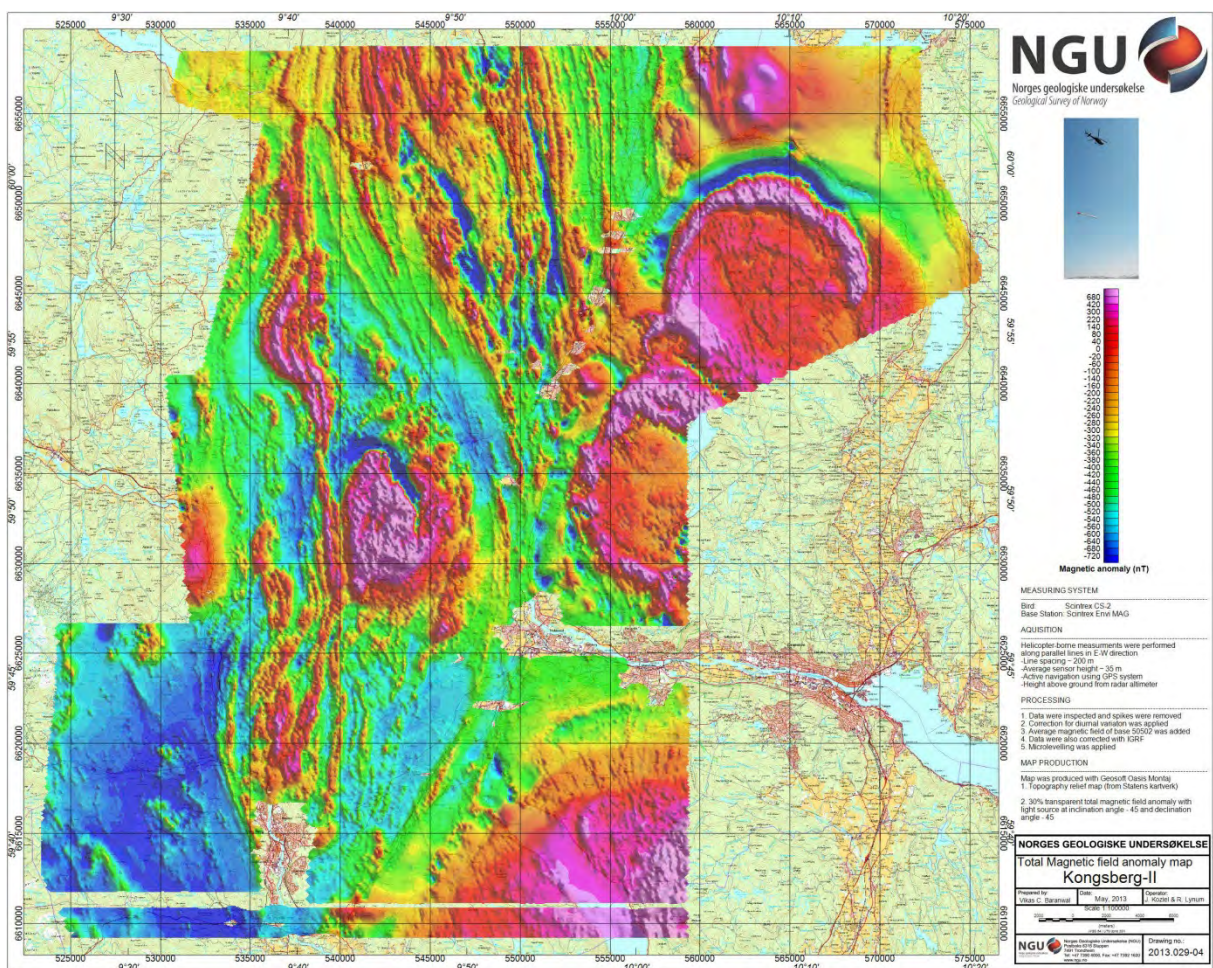


Figure 6: Total magnetic field anomaly map of Kongsberg-II area.



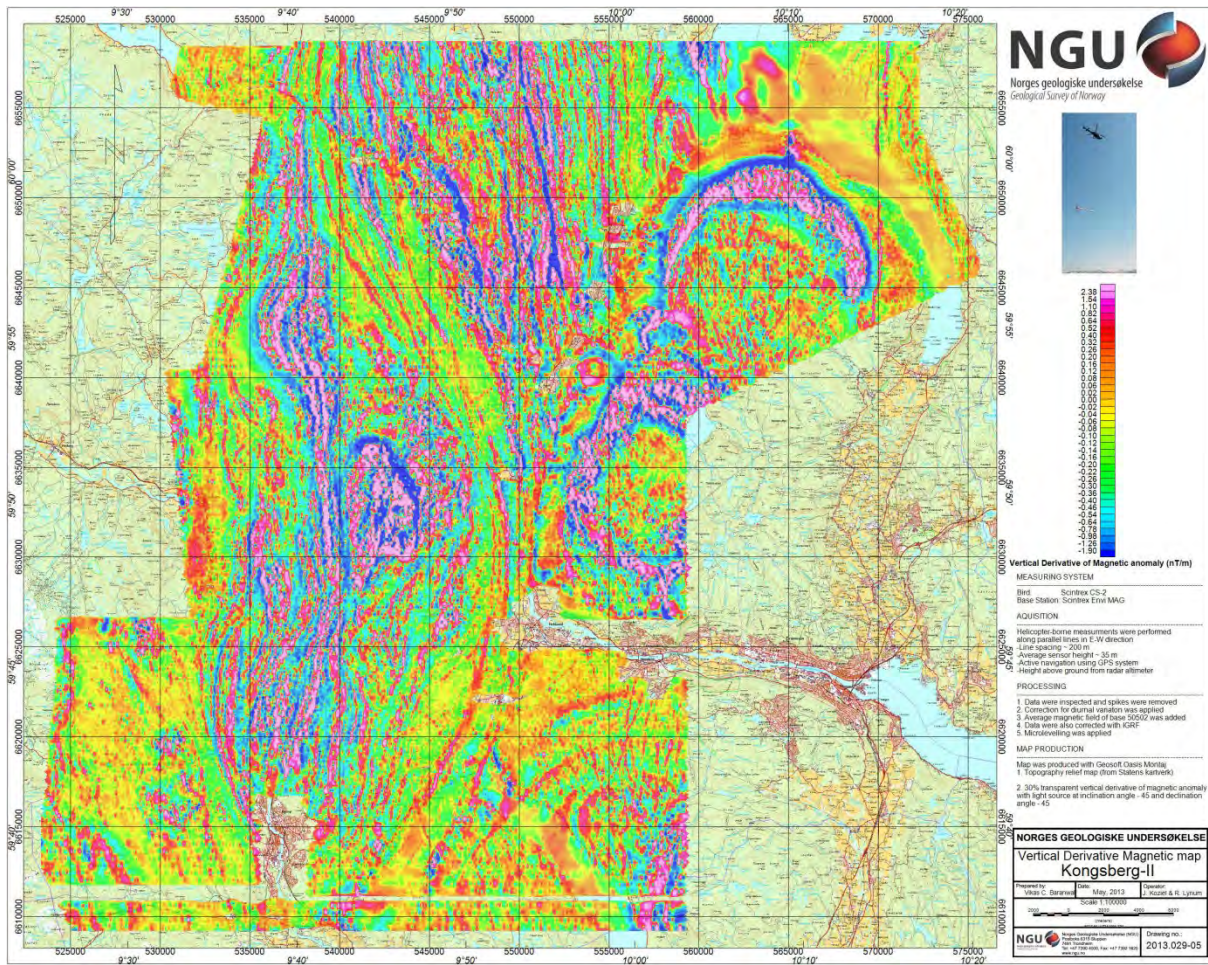


Figure 7: First vertical derivative magnetic map of Kongsberg-II area.



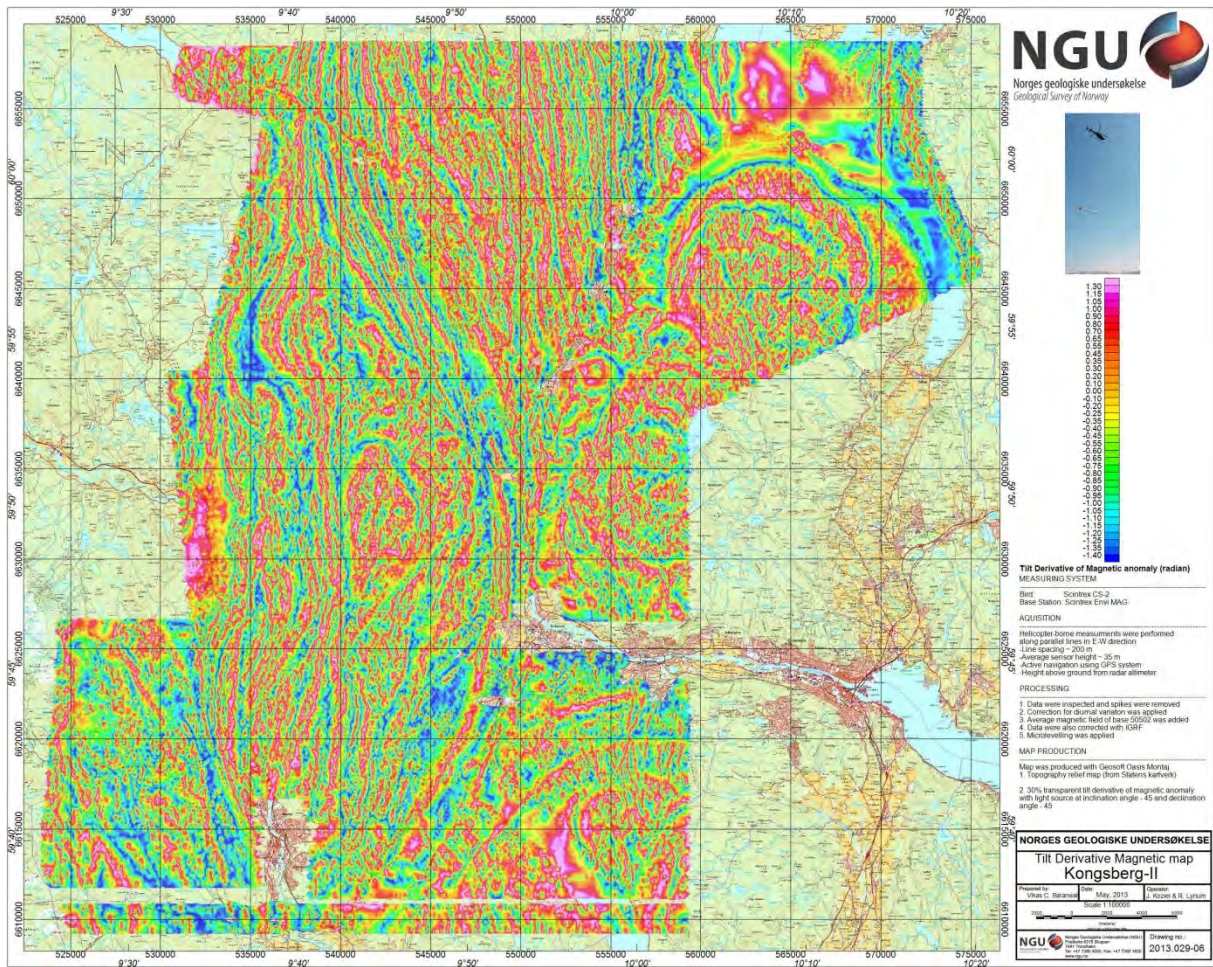


Figure 8: Tilt derivative magnetic map of Kongsberg-II area.



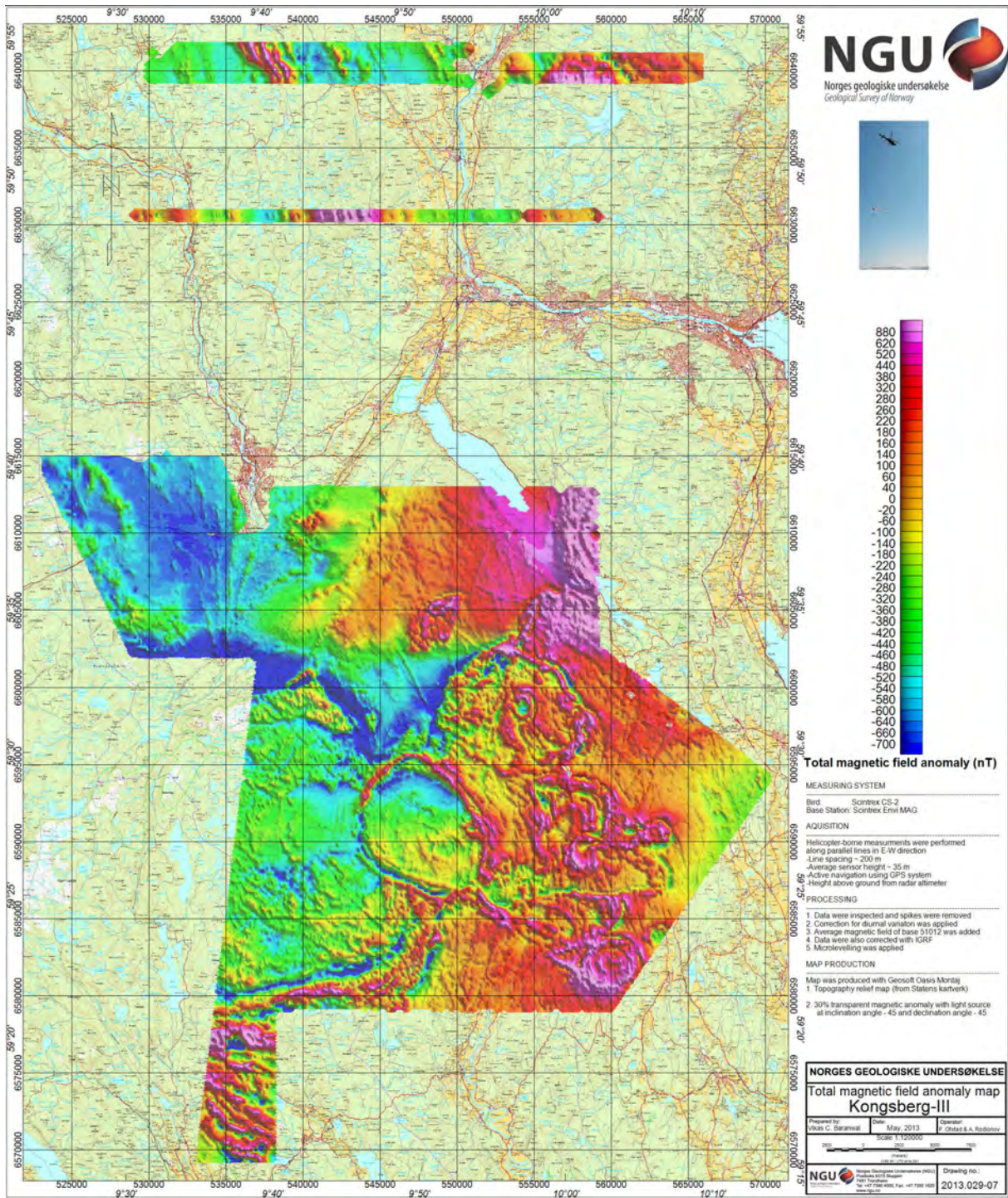


Figure 9: Total magnetic field anomaly map of Kongsberg-III area.



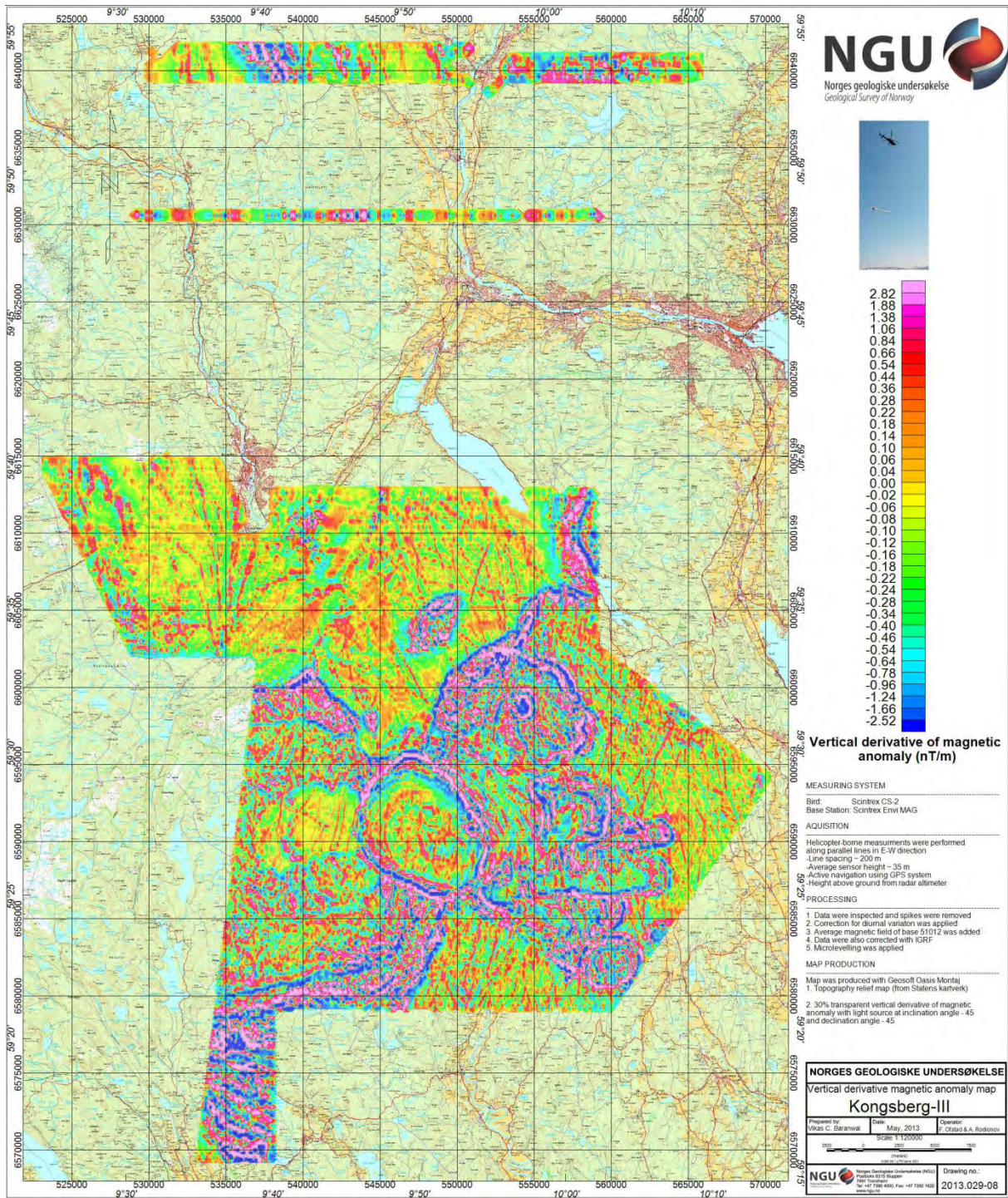


Figure 10: First vertical derivative magnetic map of Kongsberg-III area.



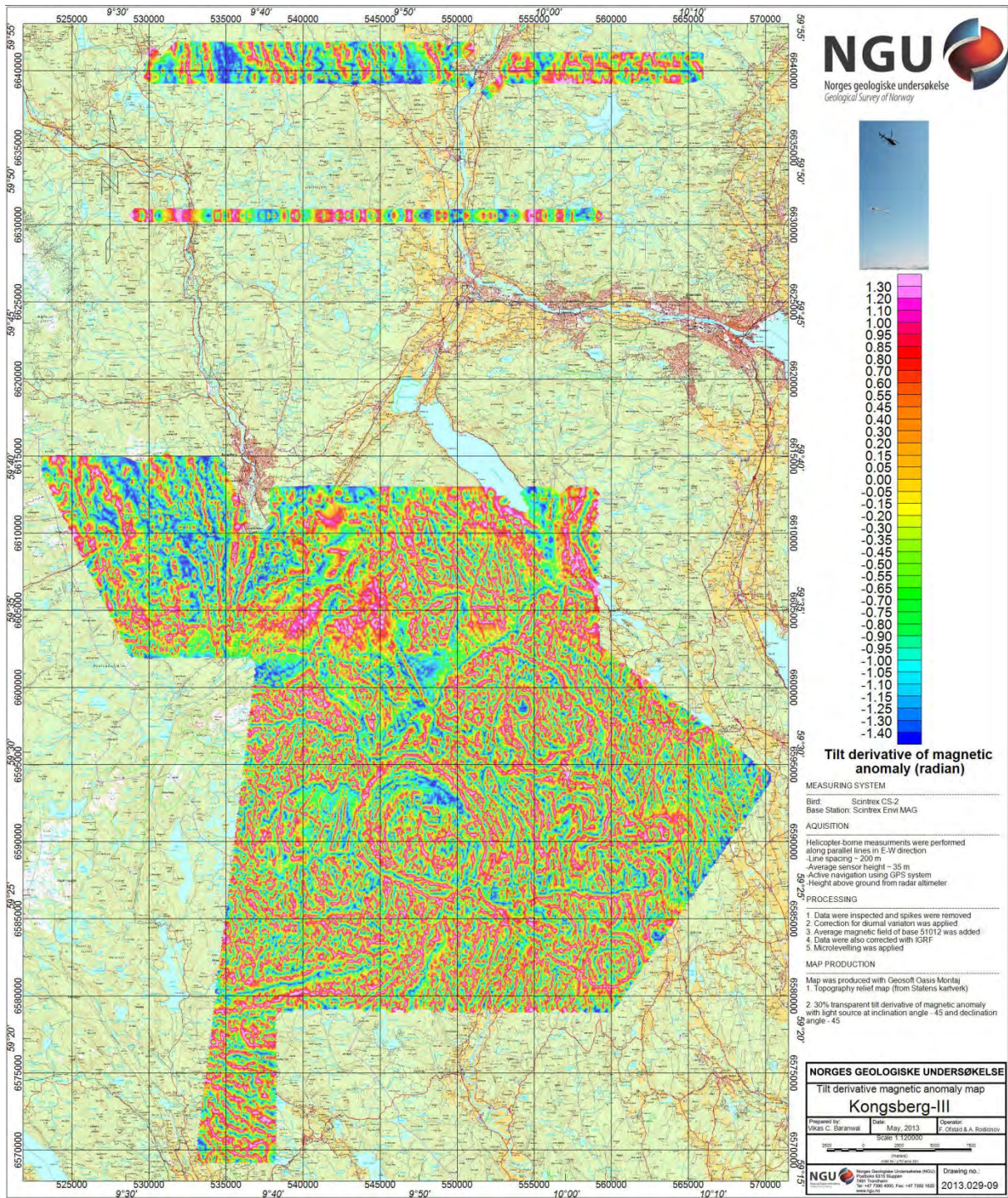


Figure 11: Tilt derivative magnetic map of Kongsberg-III area.



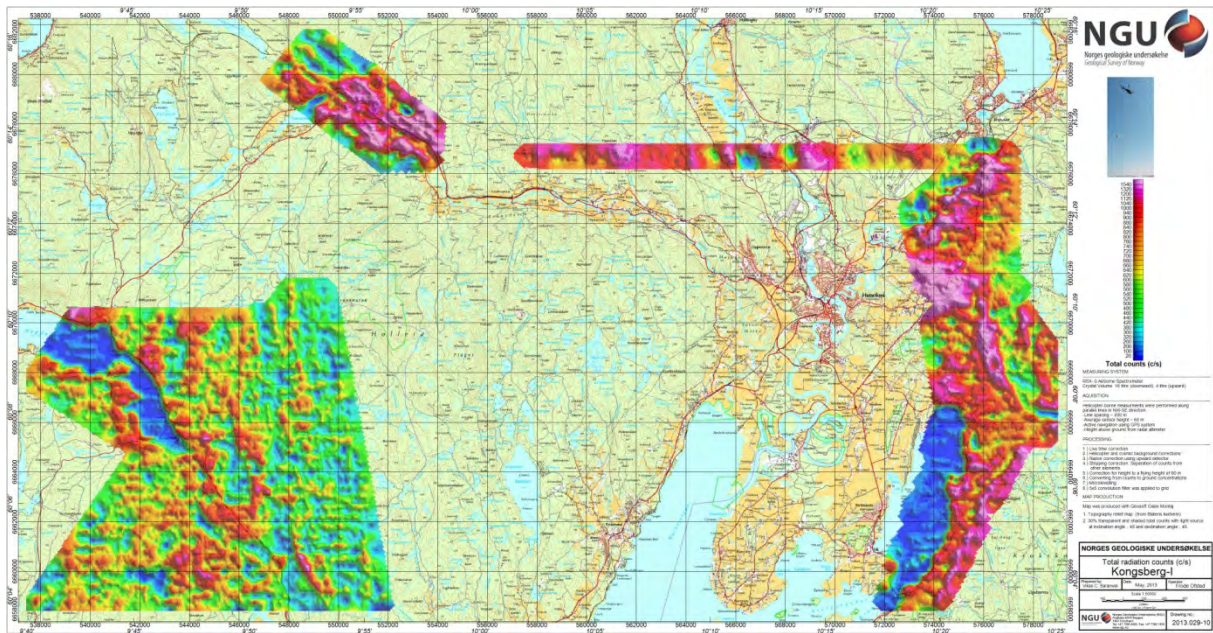


Figure 12: Total radiation count map of Kongsberg-I area.

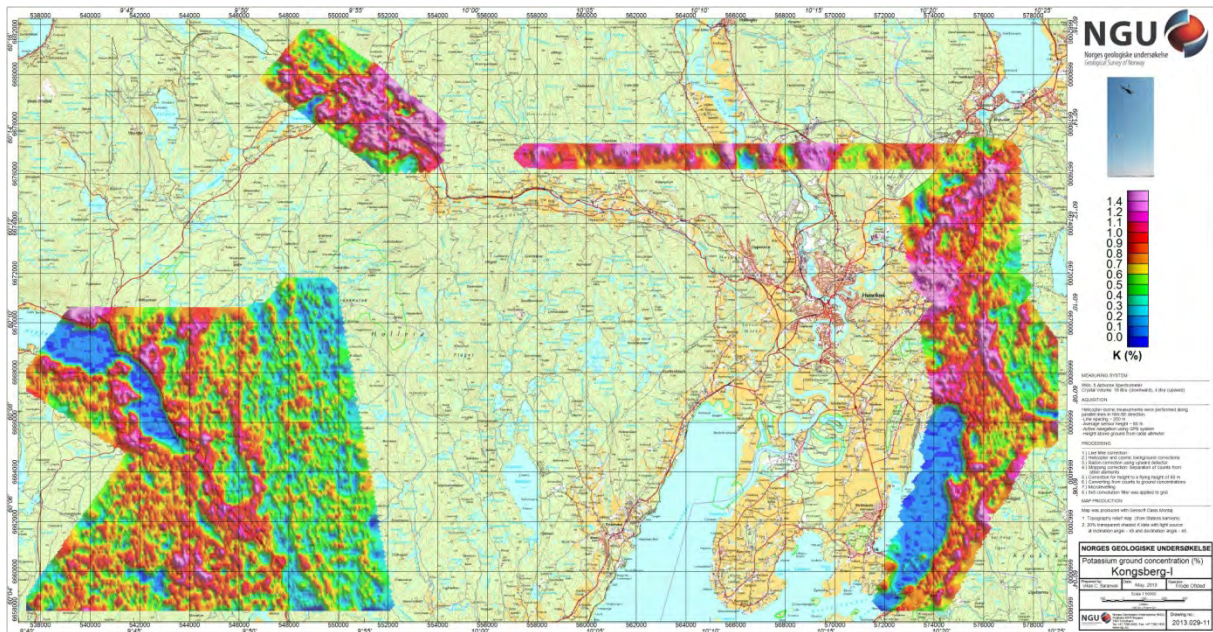


Figure 13: Ground concentration map of potassium from Kongsberg-I.



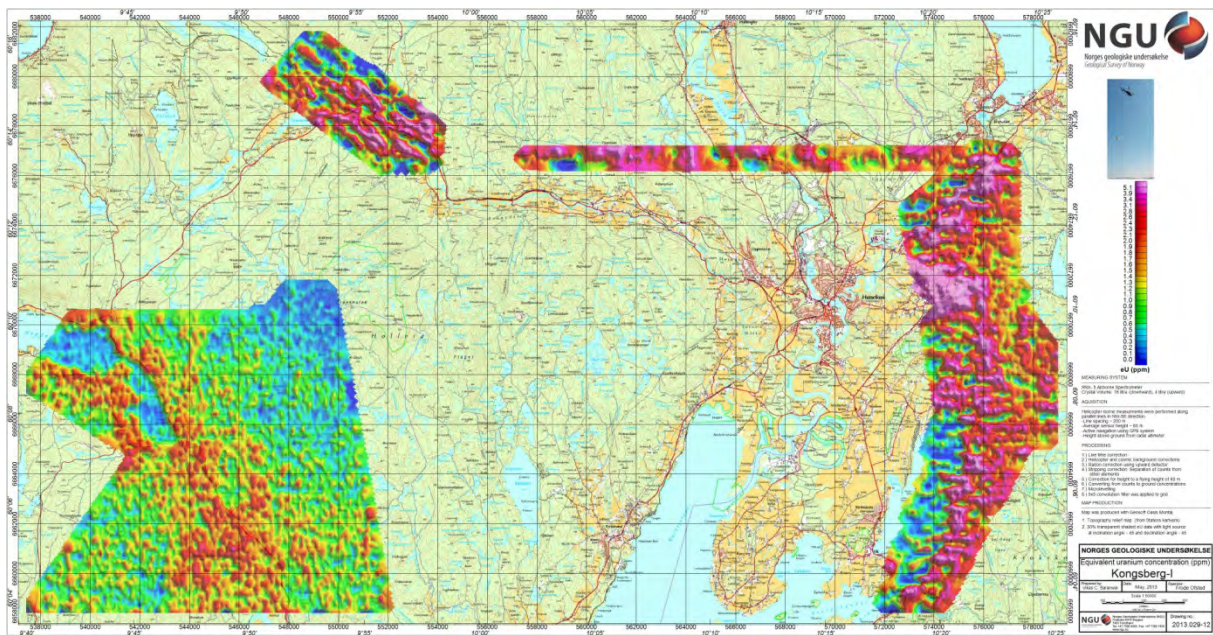


Figure 14: Ground concentration map of equivalent uranium from Kongsberg-I.

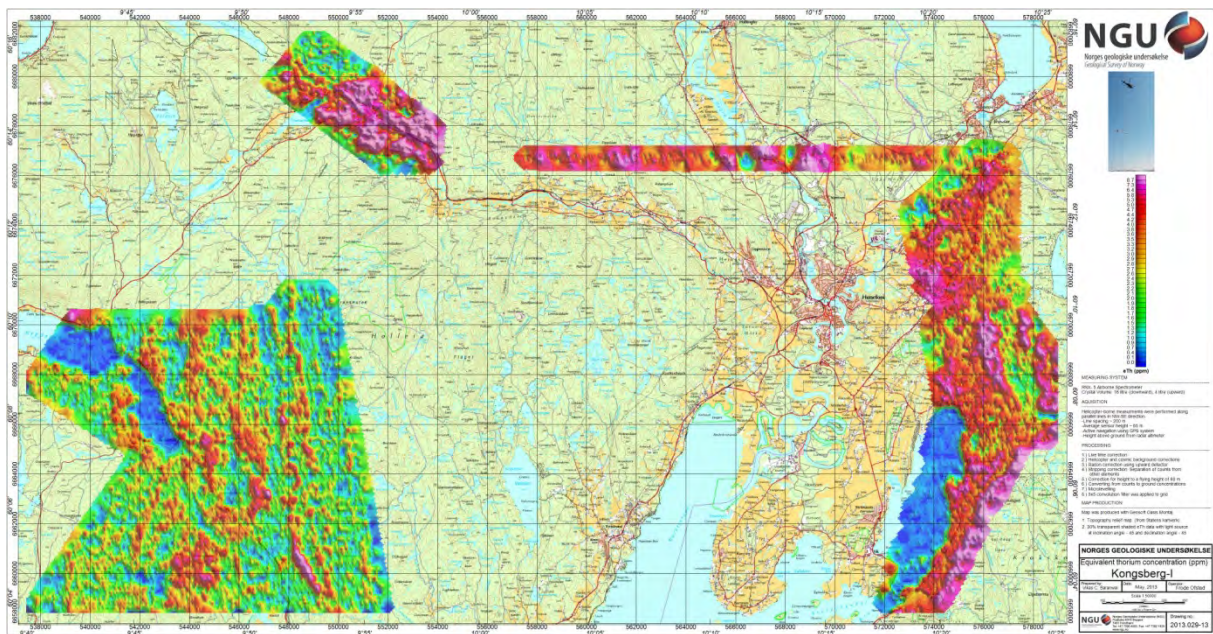


Figure 15: Ground concentration map of equivalent thorium from Kongsberg-I.



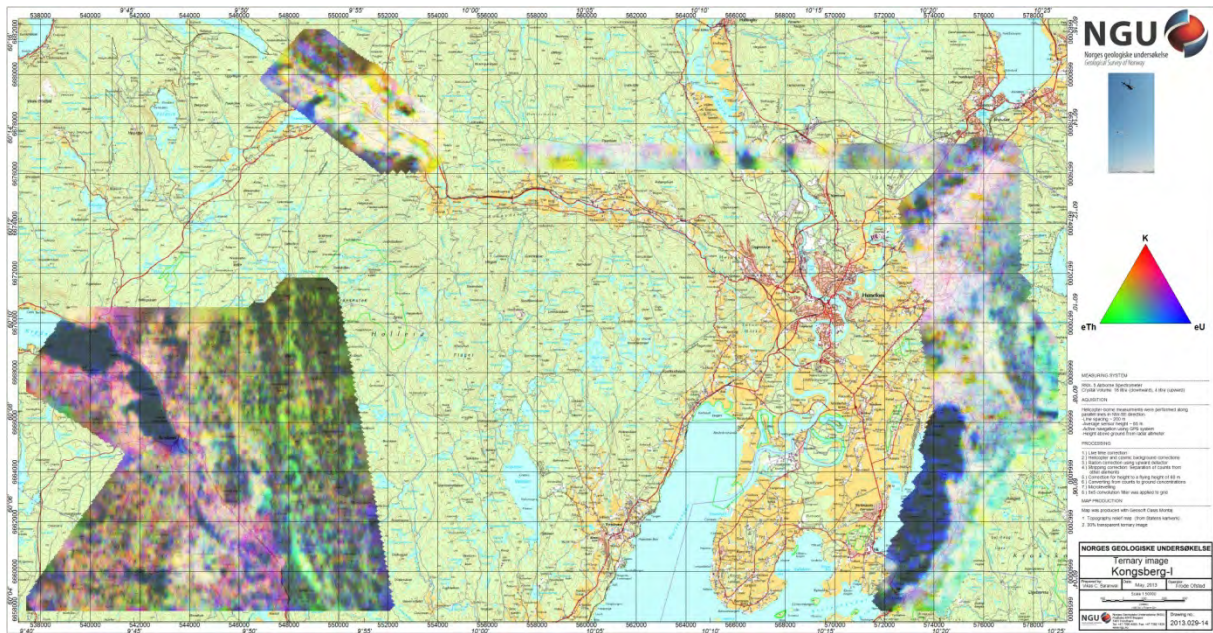


Figure 16: Ternary radiation map from Kongsberg-I.

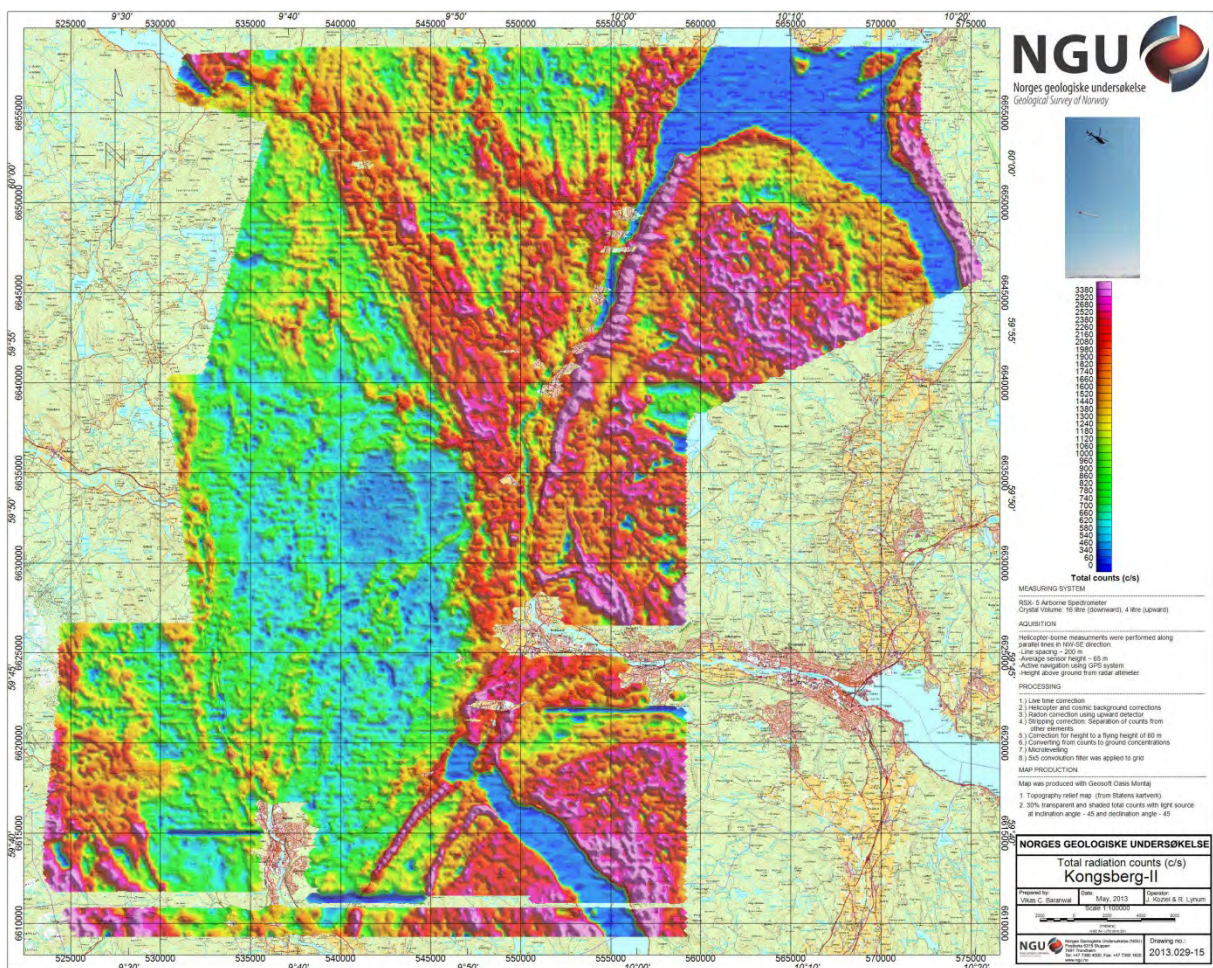


Figure 17: Total radiation count map from Kongsberg-II.



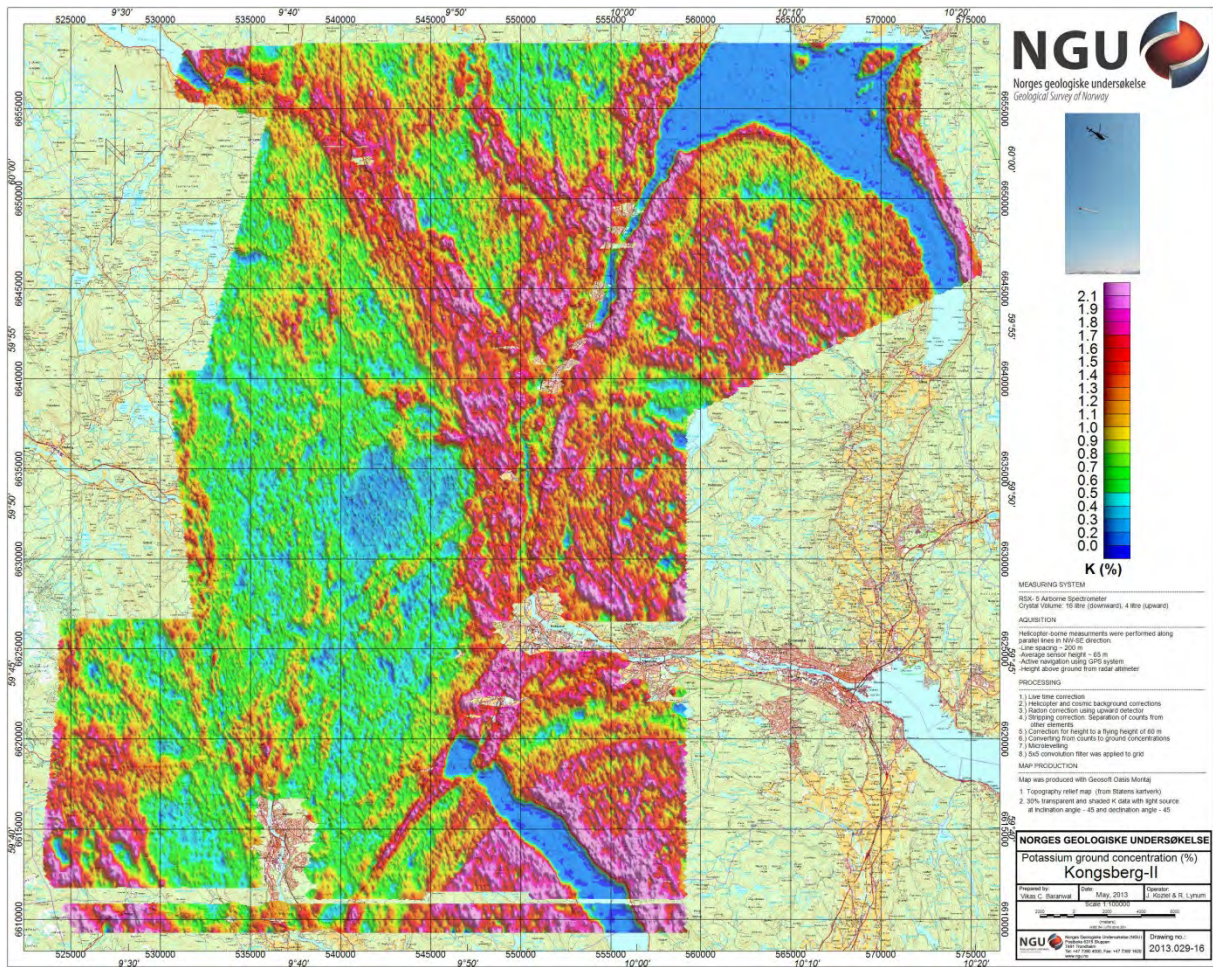


Figure 18: Ground concentration map of potassium from Kongsberg-II.



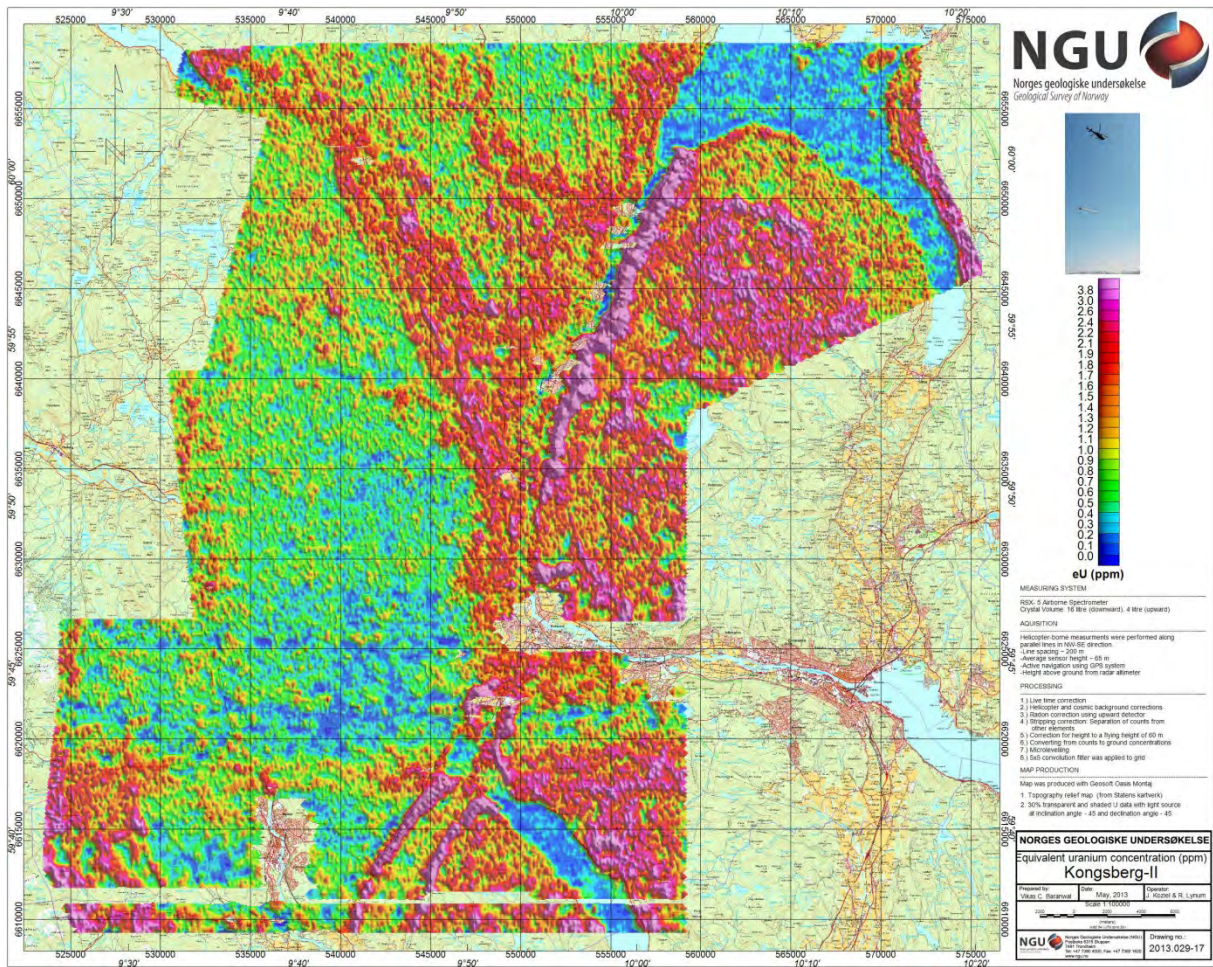


Figure 19: Ground concentration map of equivalent uranium from Kongsberg-II.



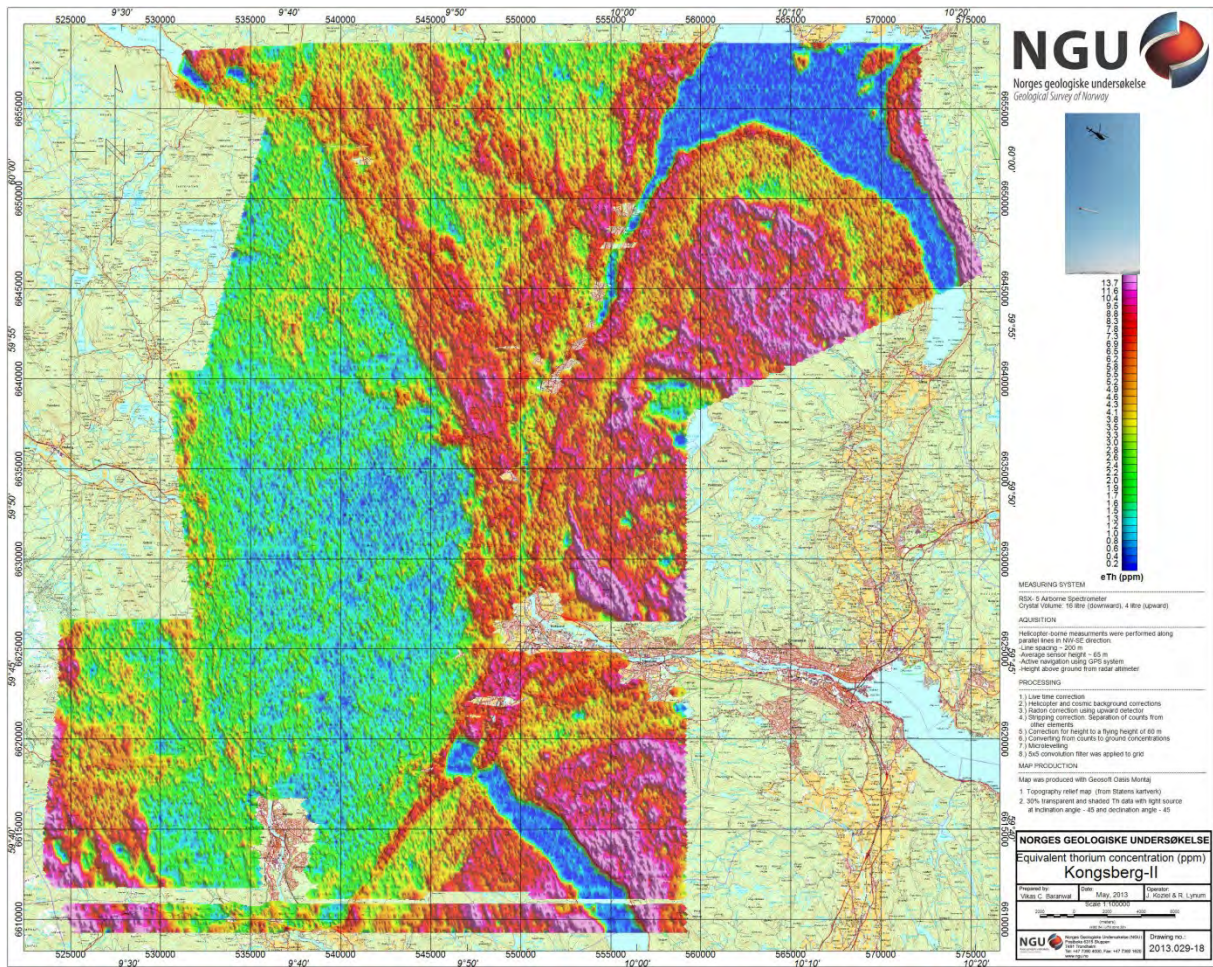


Figure 20: Ground concentration map of equivalent thorium from Kongsberg-II.



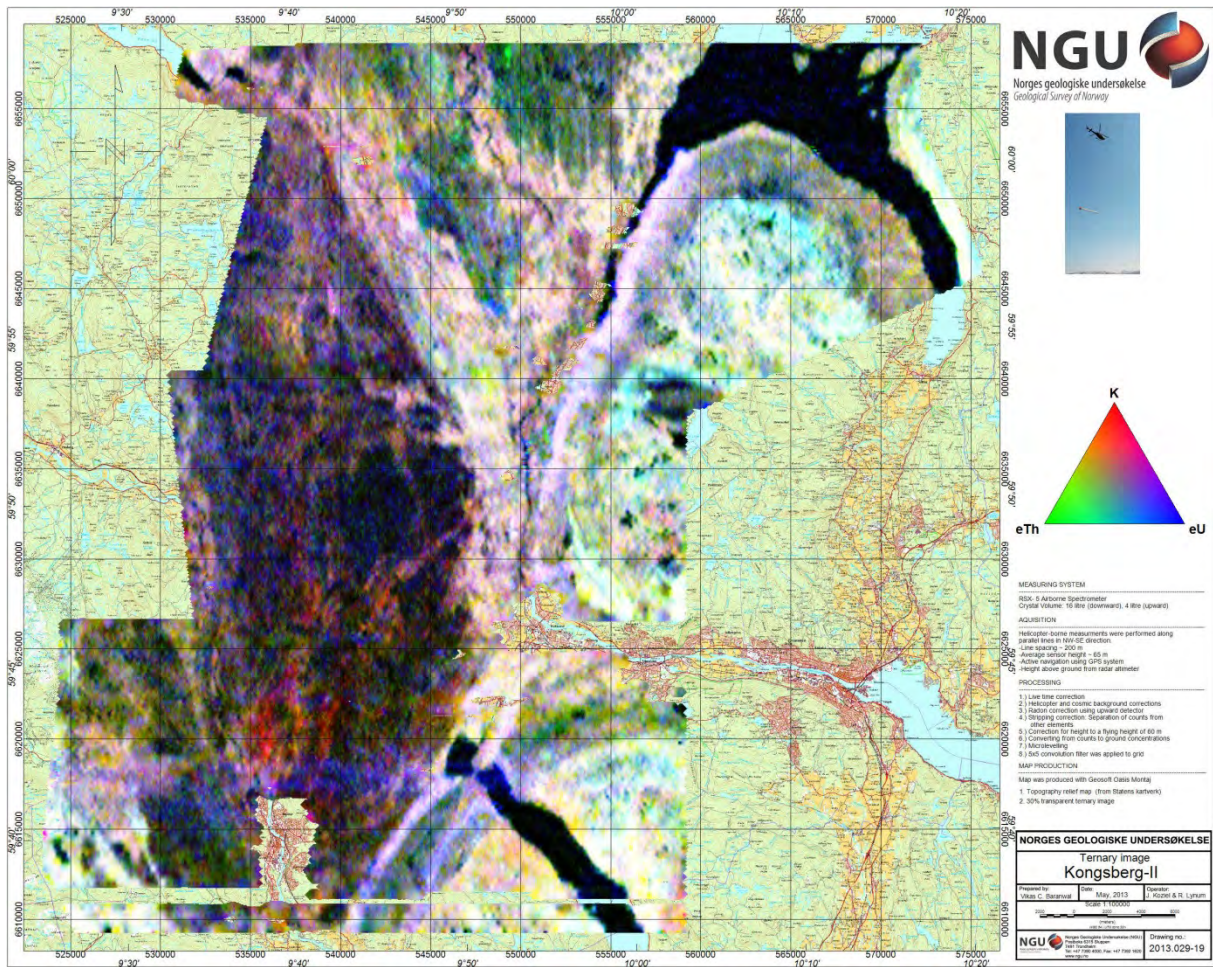


Figure 21: Ternary radiation map from Kongsberg-II.



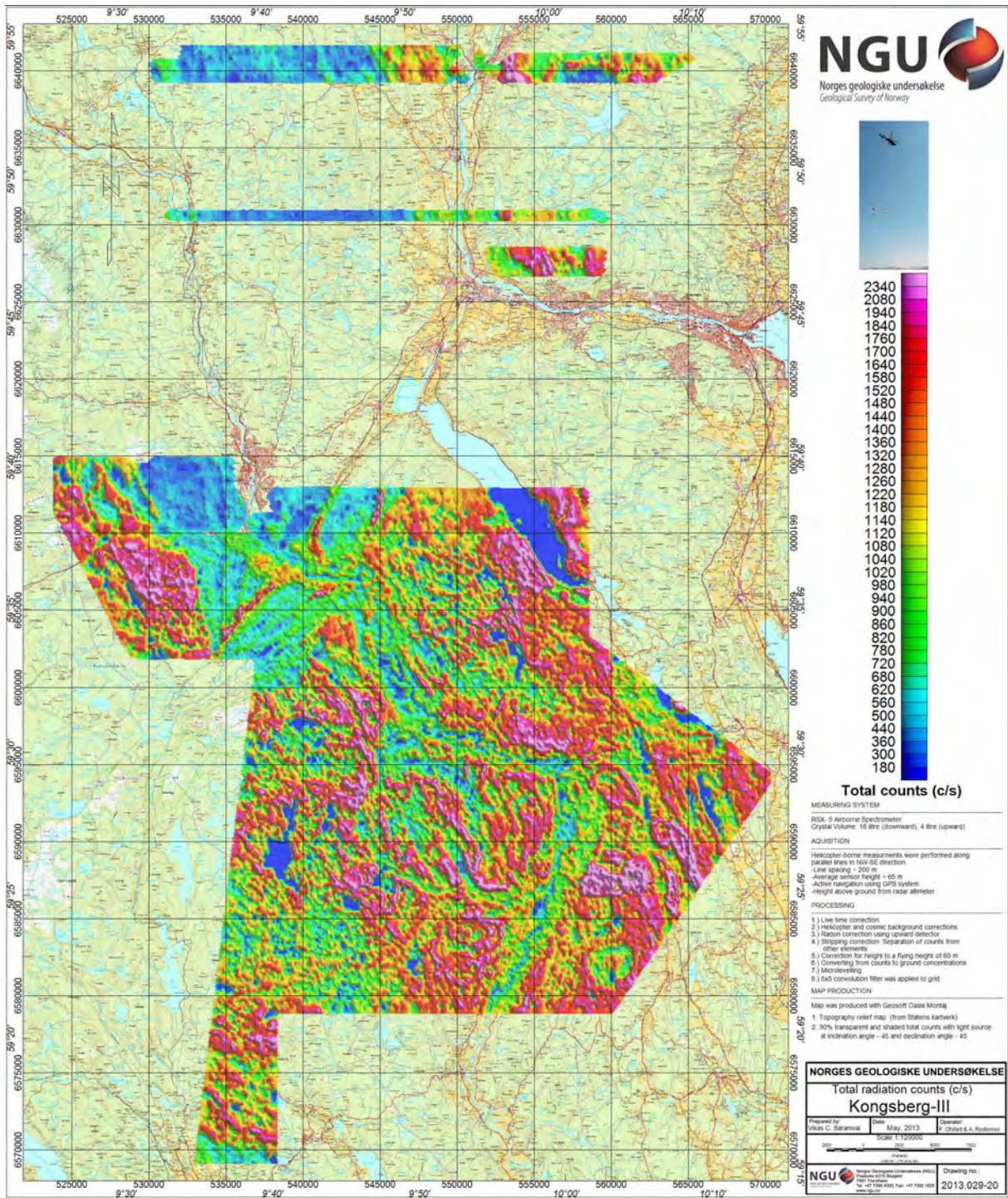


Figure 22: Total radiation count map from Kongsberg-III.



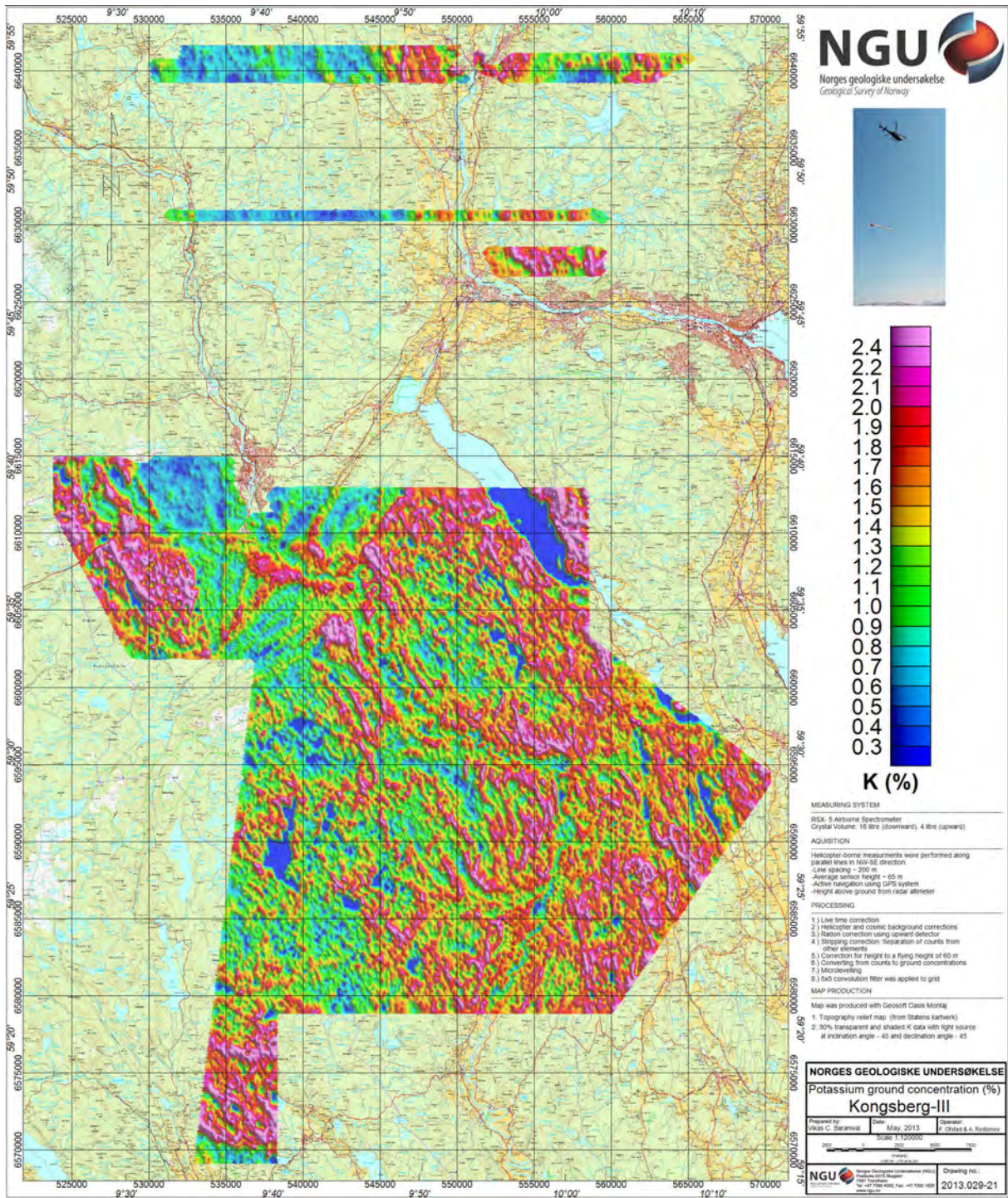


Figure 23: Ground concentration map of potassium from Kongsberg-III.



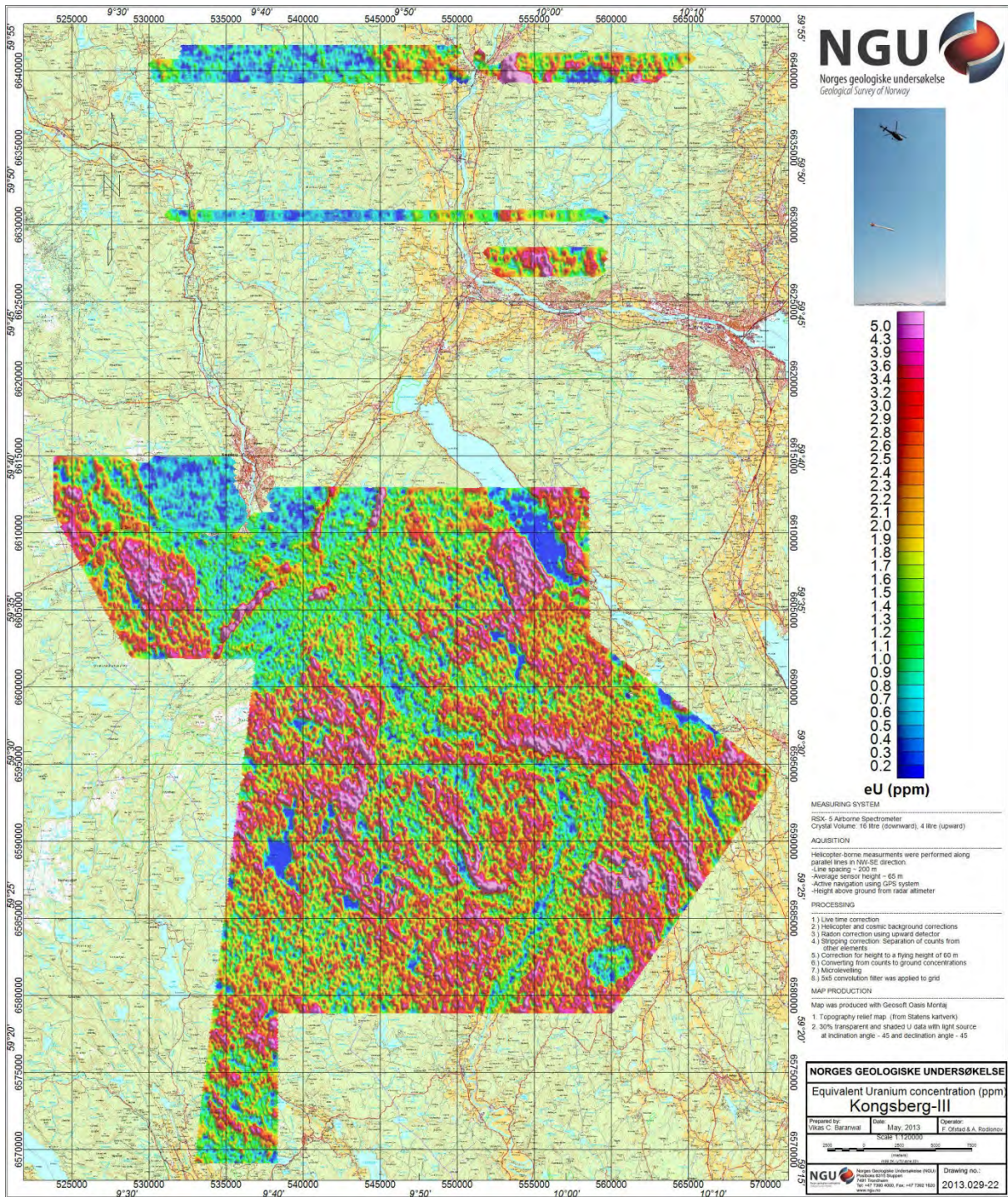


Figure 24: Ground concentration map of equivalent uranium from Kongsberg-III.



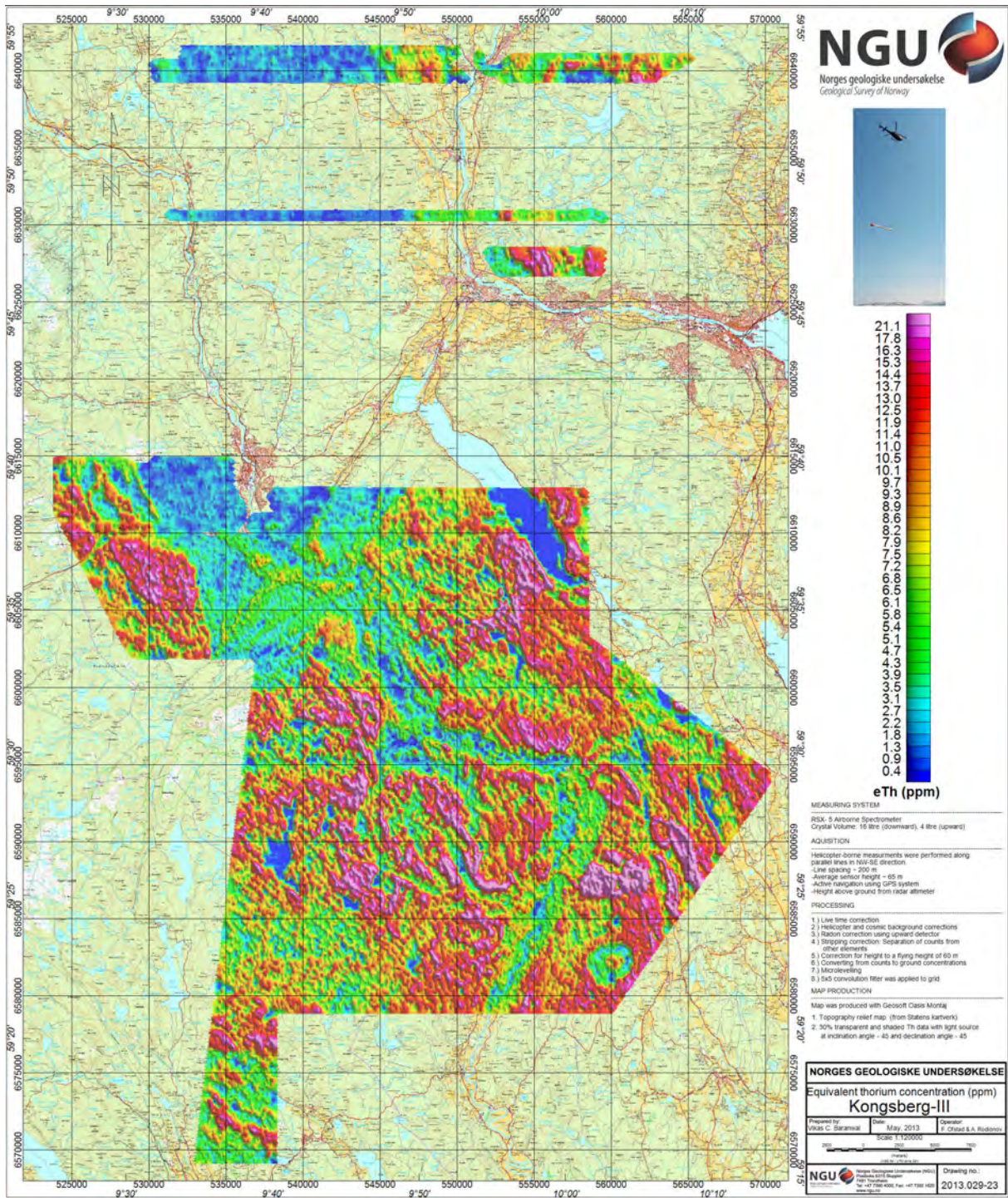


Figure 25: Ground concentration map of equivalent thorium from Kongsberg-III.



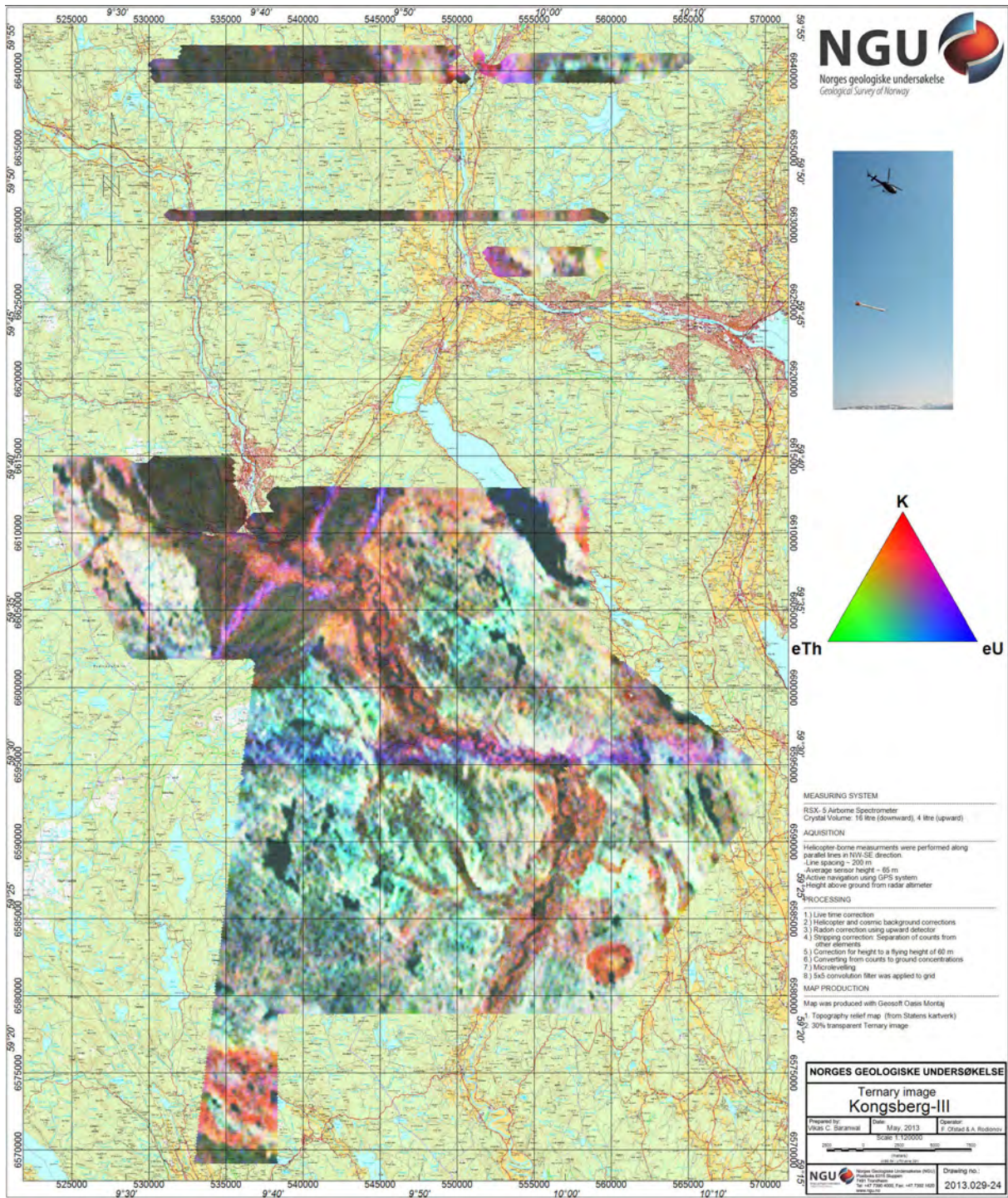


Figure 26: Ternary radiation map from Kongsberg-I.



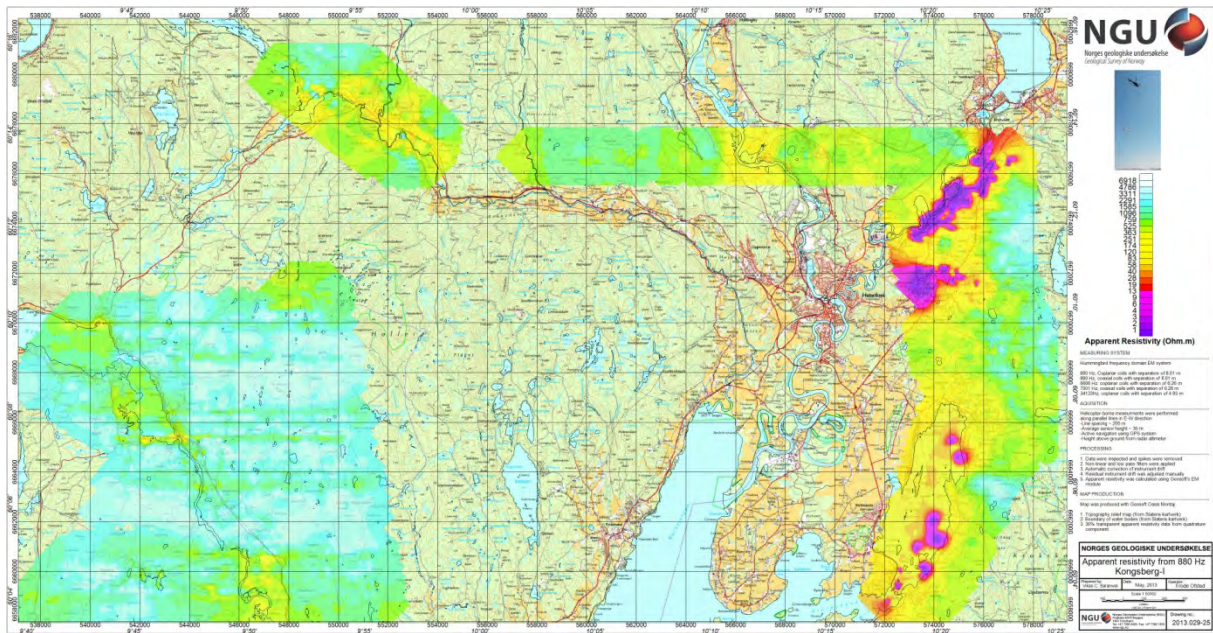


Figure 27: Apparent resistivity map from frequency 880 Hz from Kongsberg-I.

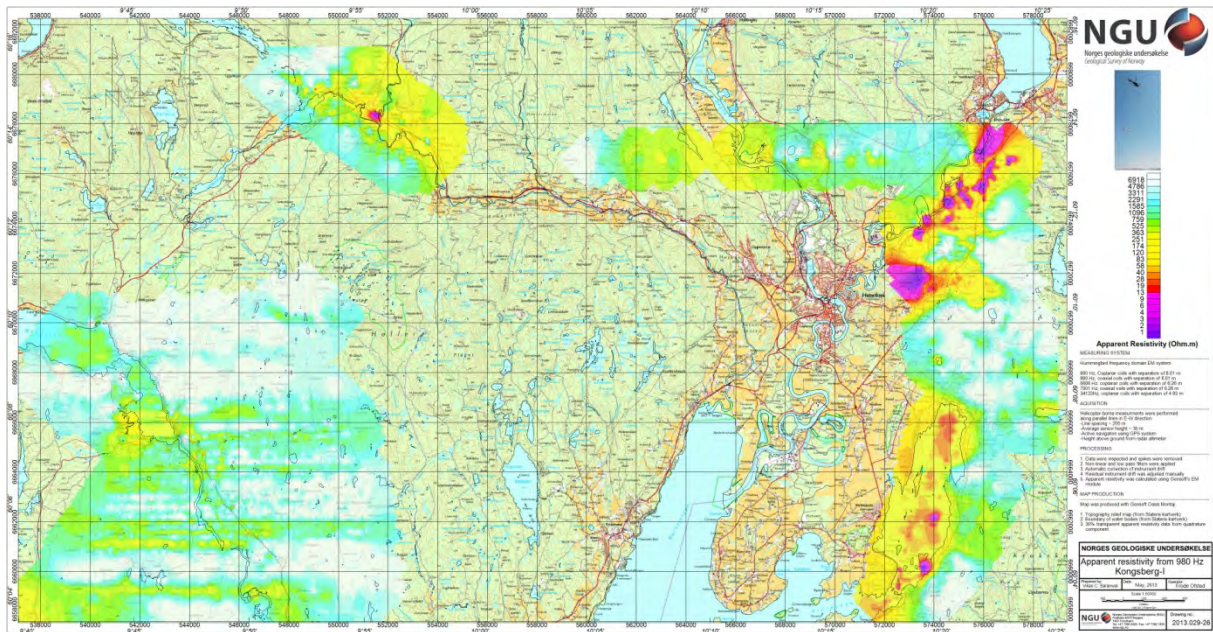


Figure 28: Apparent resistivity map from frequency 980 Hz from Kongsberg-I.



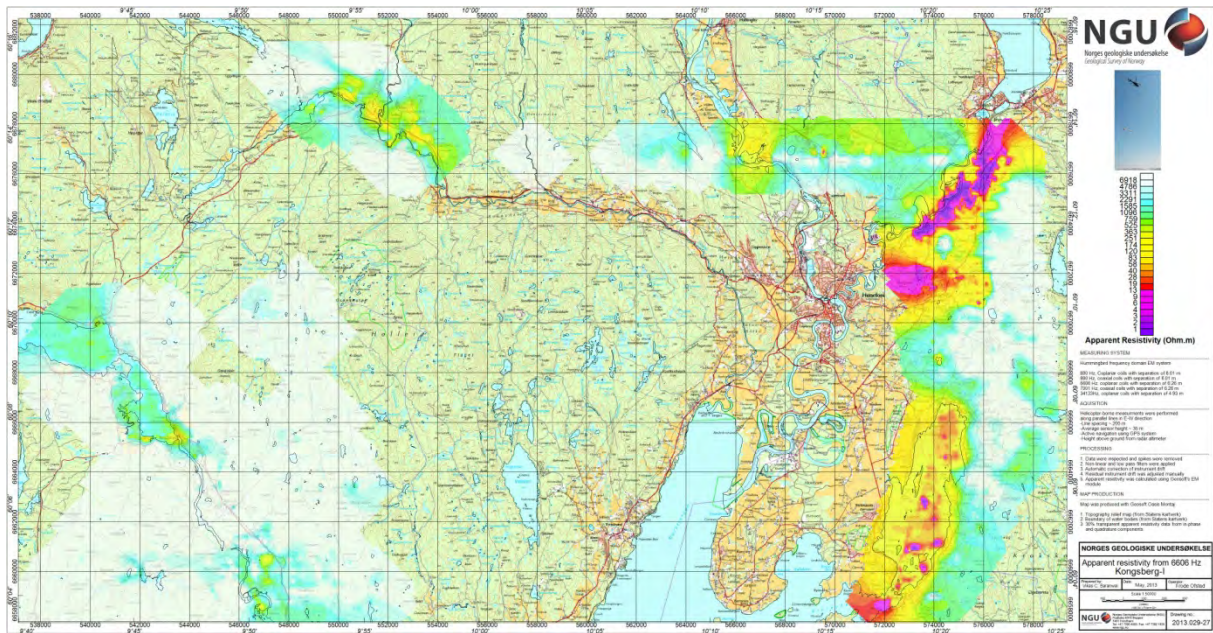


Figure 29: Apparent resistivity map from frequency 6606 Hz from Kongsberg-I.

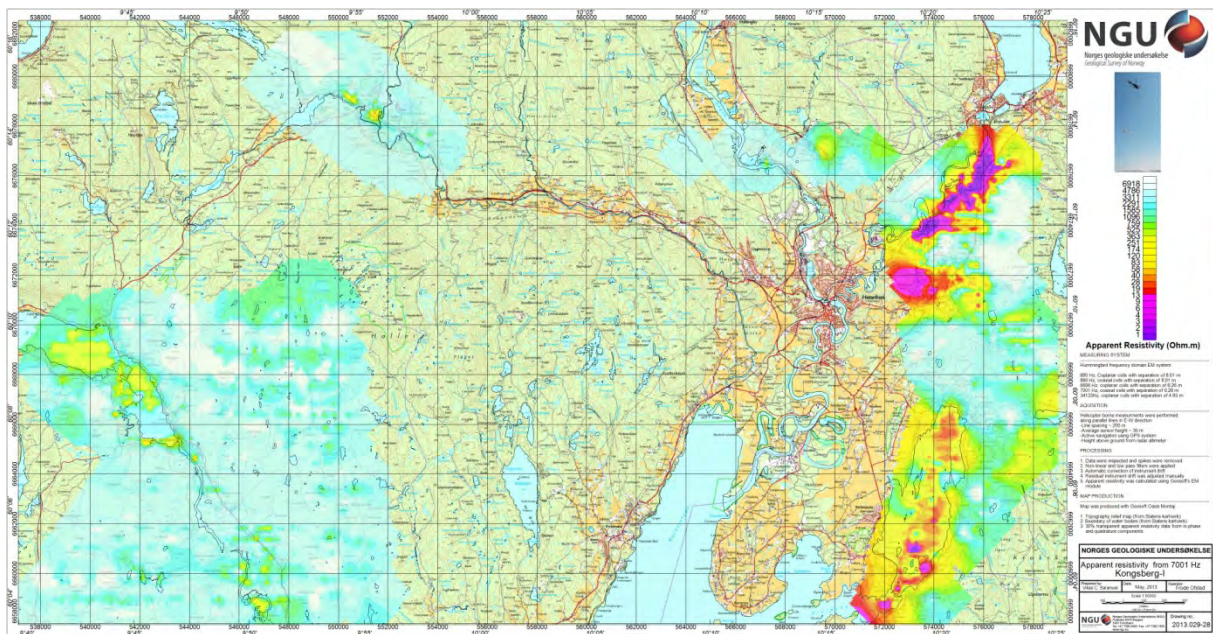


Figure 30: Apparent resistivity map from frequency 7001 Hz from Kongsberg-I.



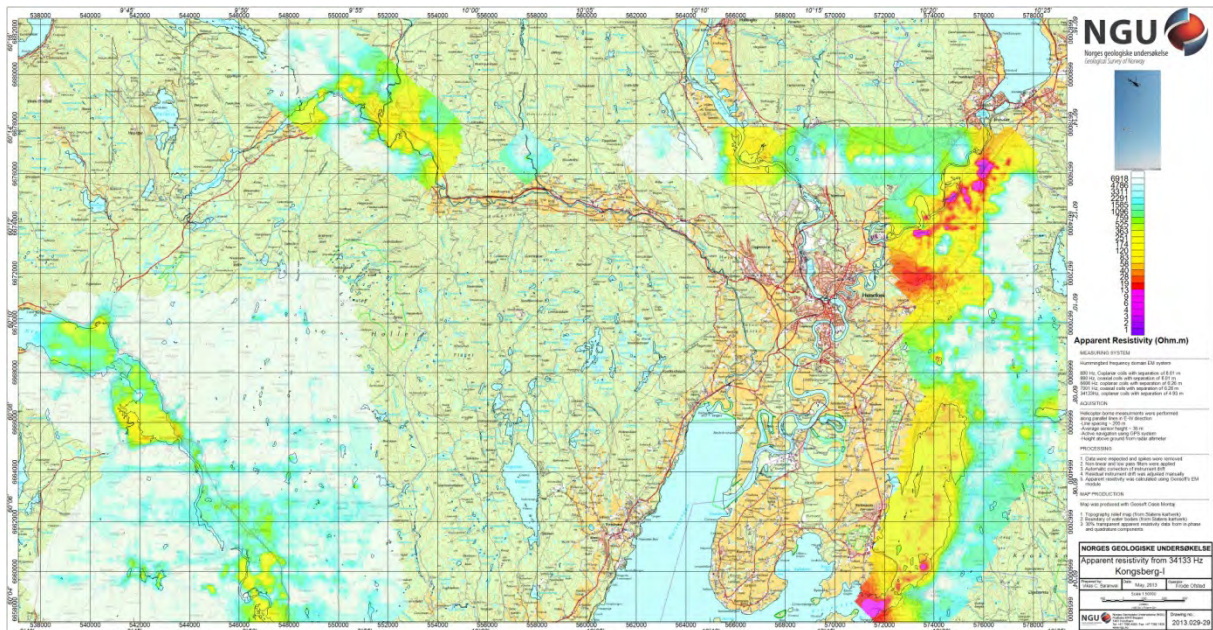


Figure 31: Apparent resistivity map from frequency 34133 Hz from Kongsberg-I.

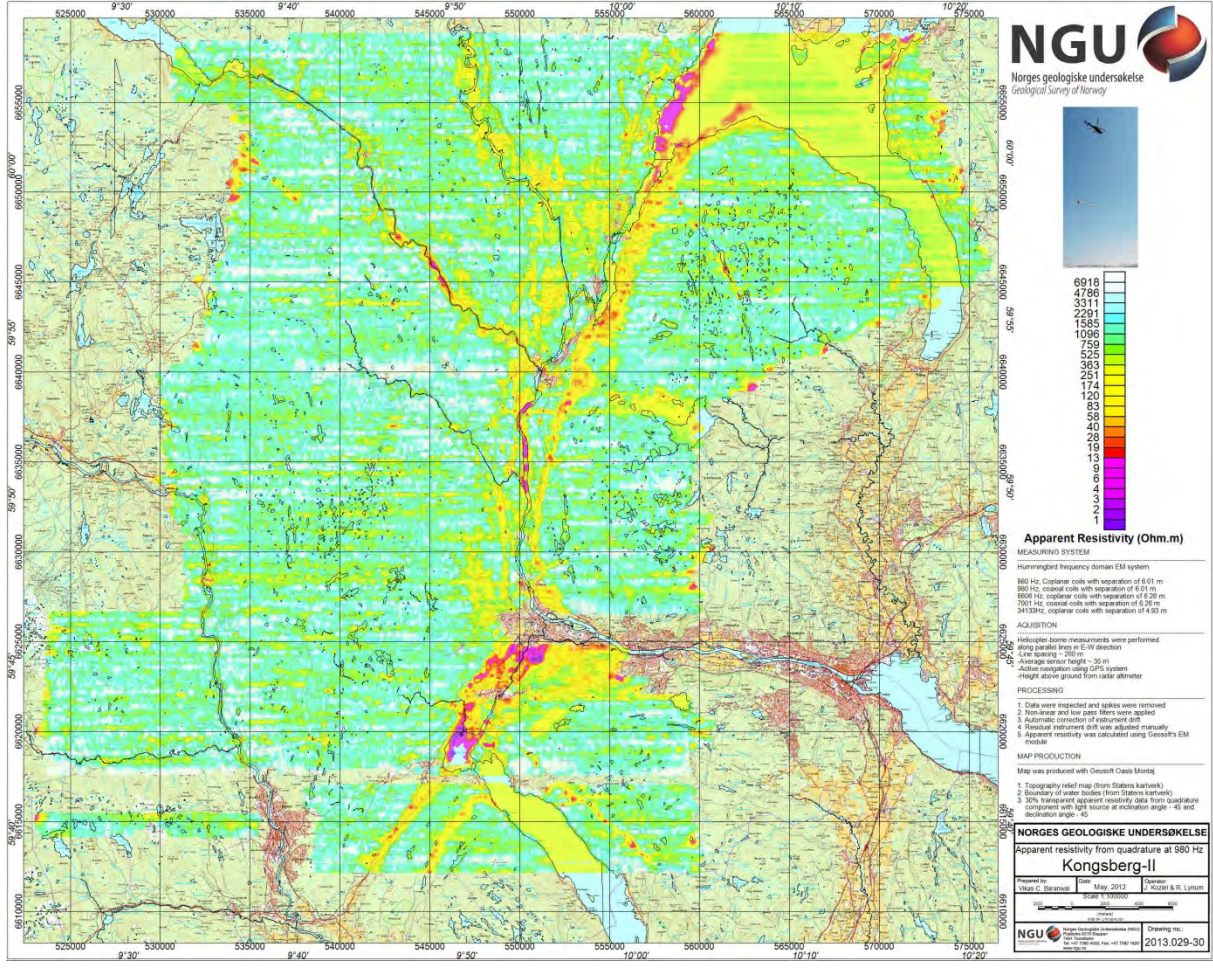


Figure 32: Apparent resistivity map from frequency 980 Hz from Kongsberg-II.



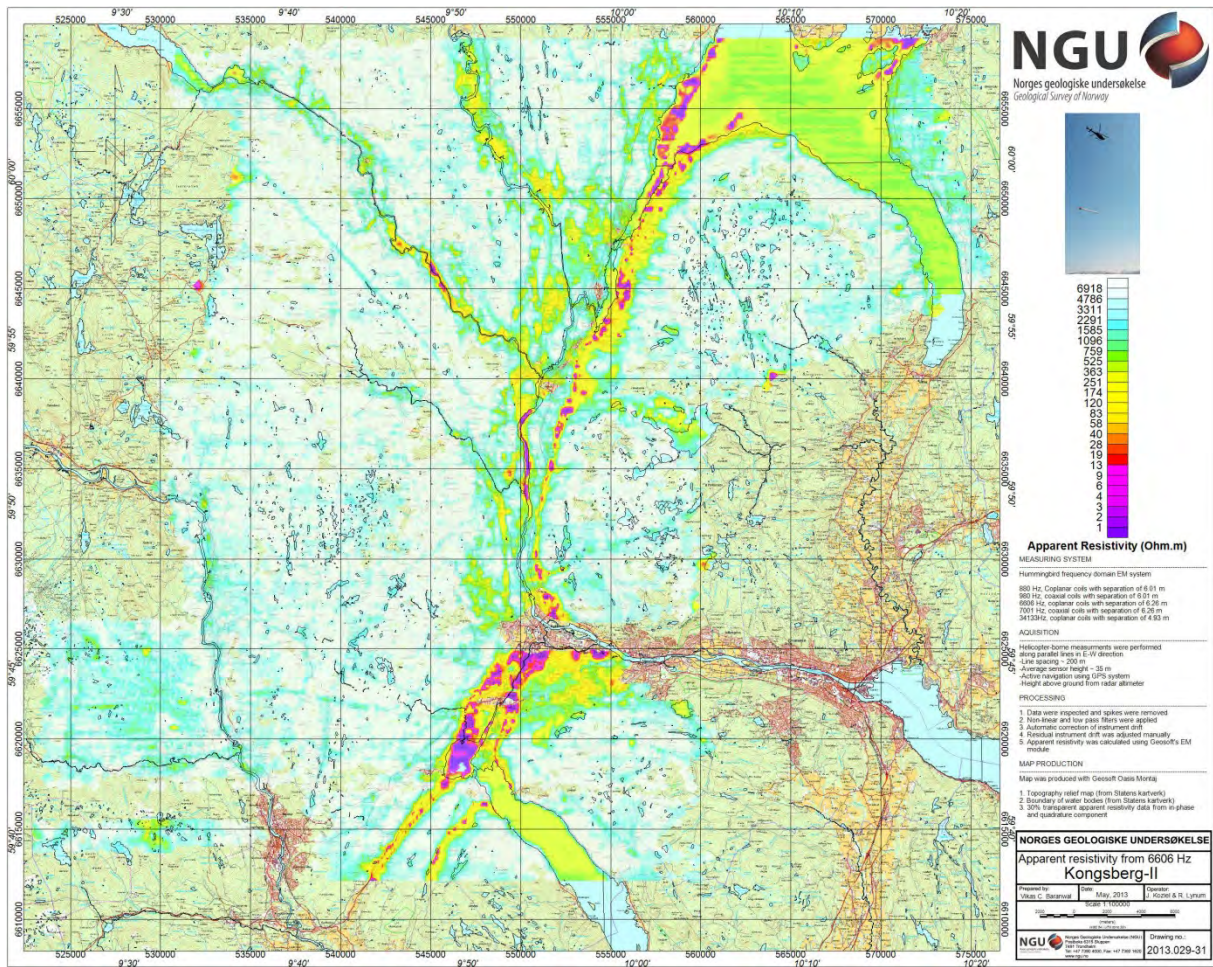


Figure 33: Apparent resistivity map from frequency 6606 Hz from Kongsberg-II.



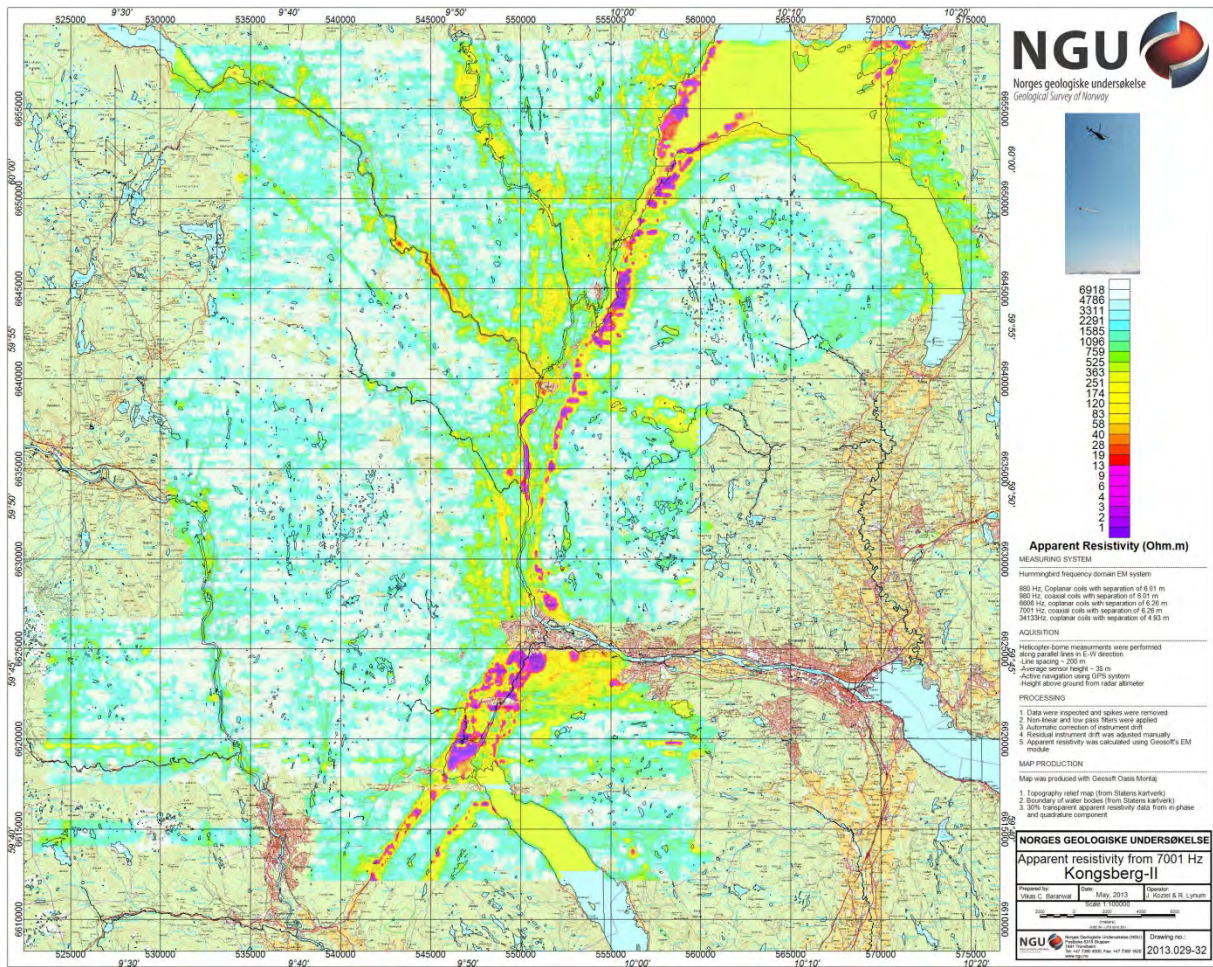


Figure 34: Apparent resistivity map from frequency 7001 Hz from Kongsberg-II.



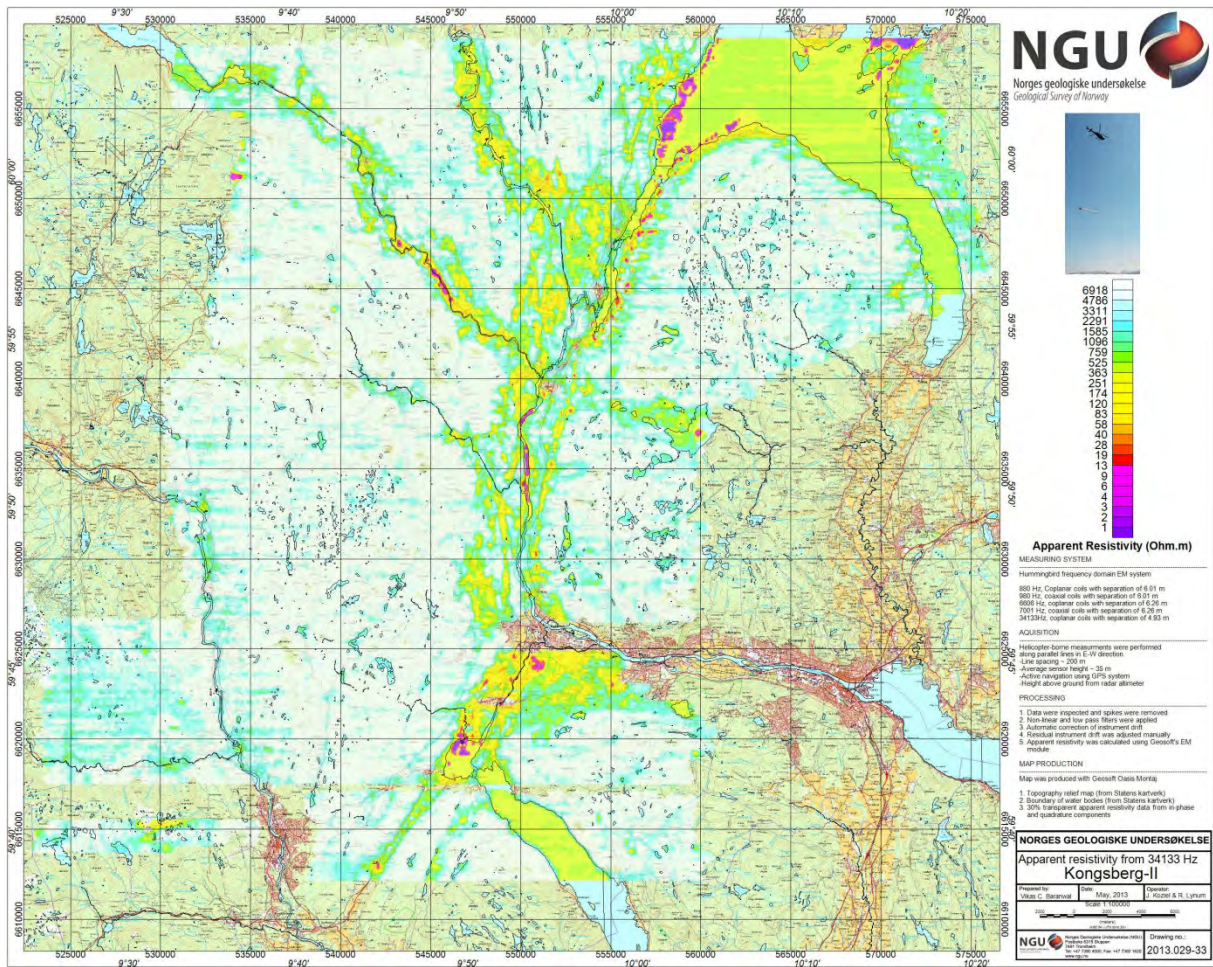


Figure 35: Apparent resistivity map from frequency 34133 Hz from Kongsberg-II.



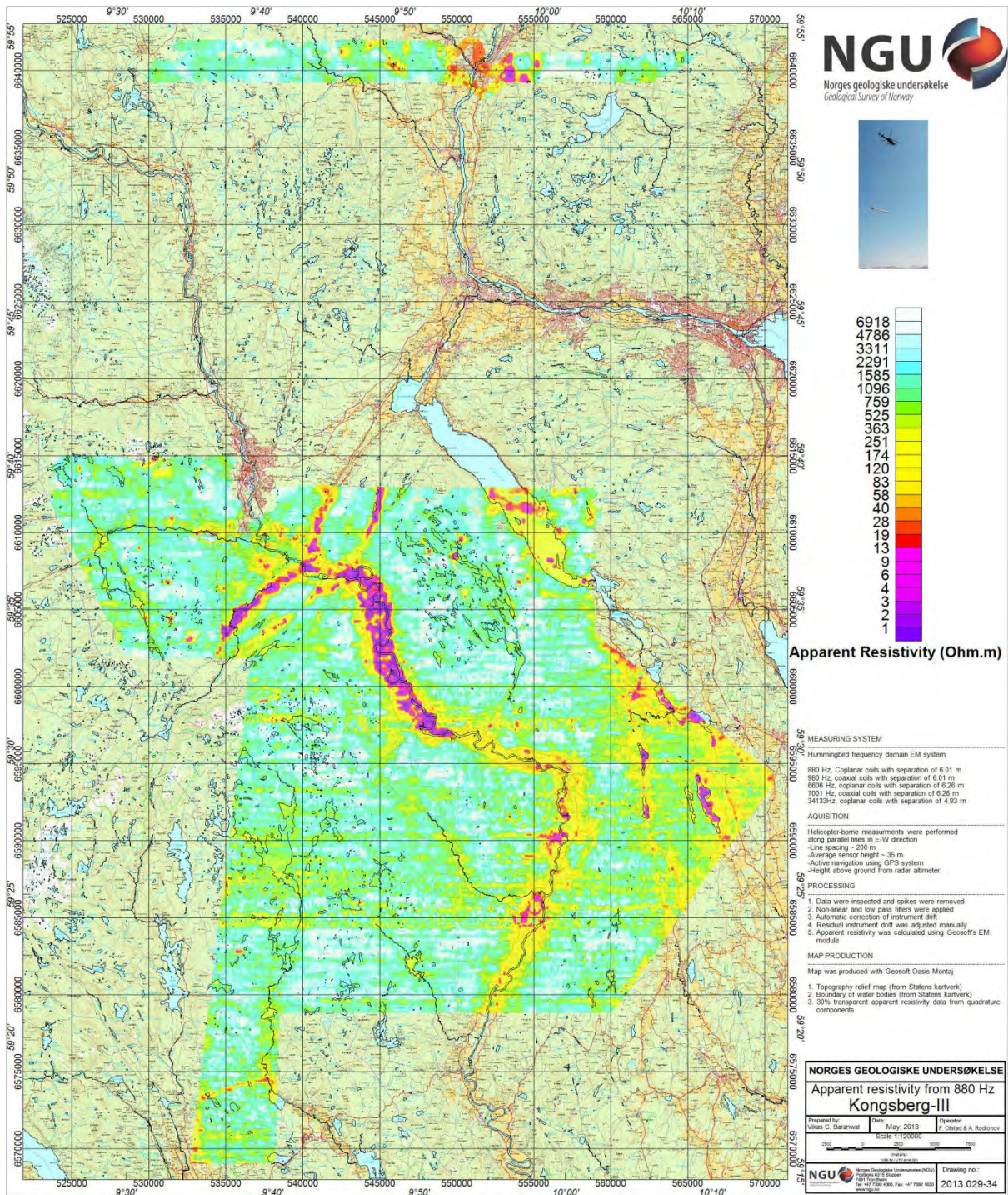


Figure 36: Apparent resistivity map from frequency 880 Hz from Kongsberg-III.



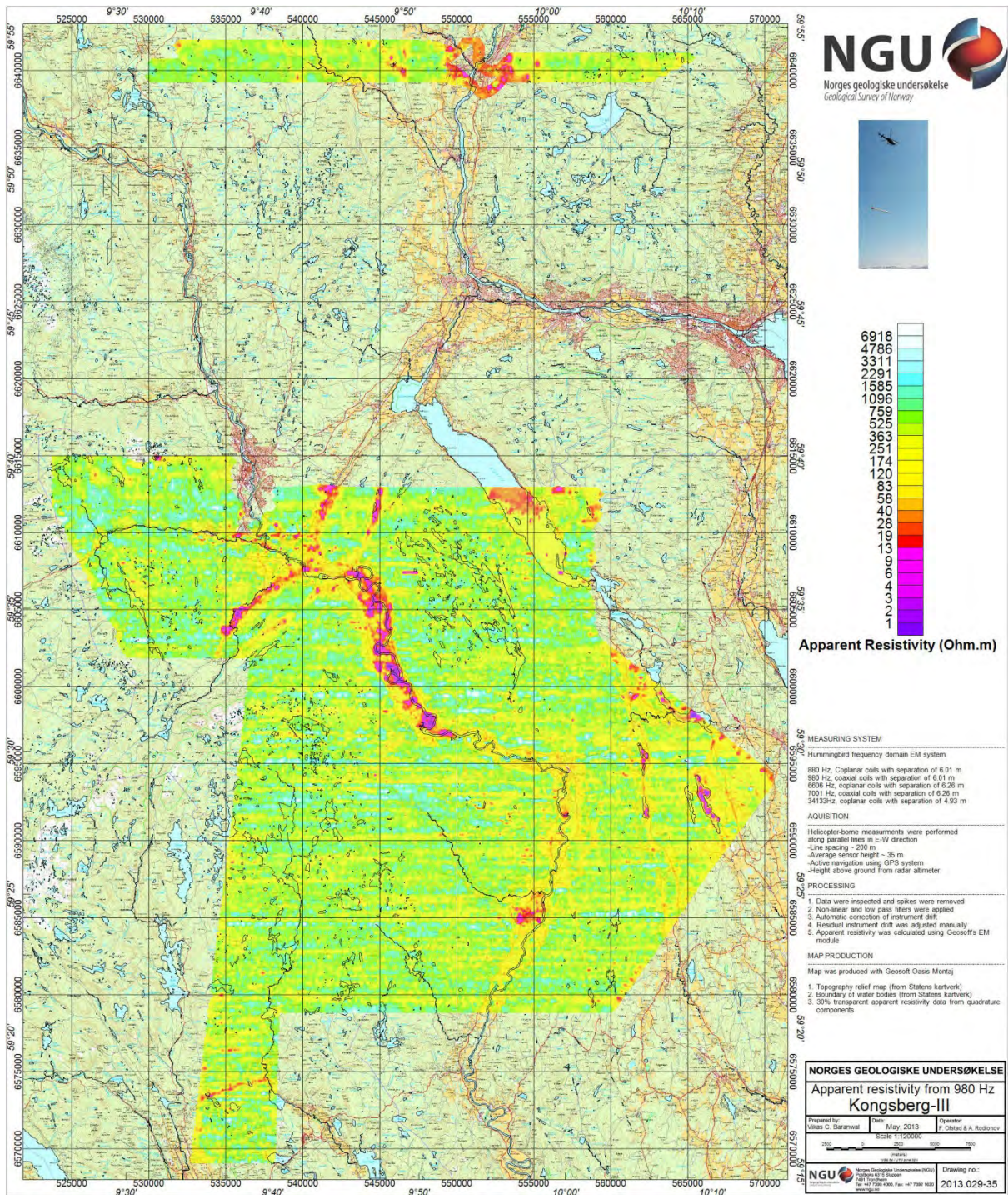


Figure 37: Apparent resistivity map from frequency 980 Hz from Kongsberg-I.



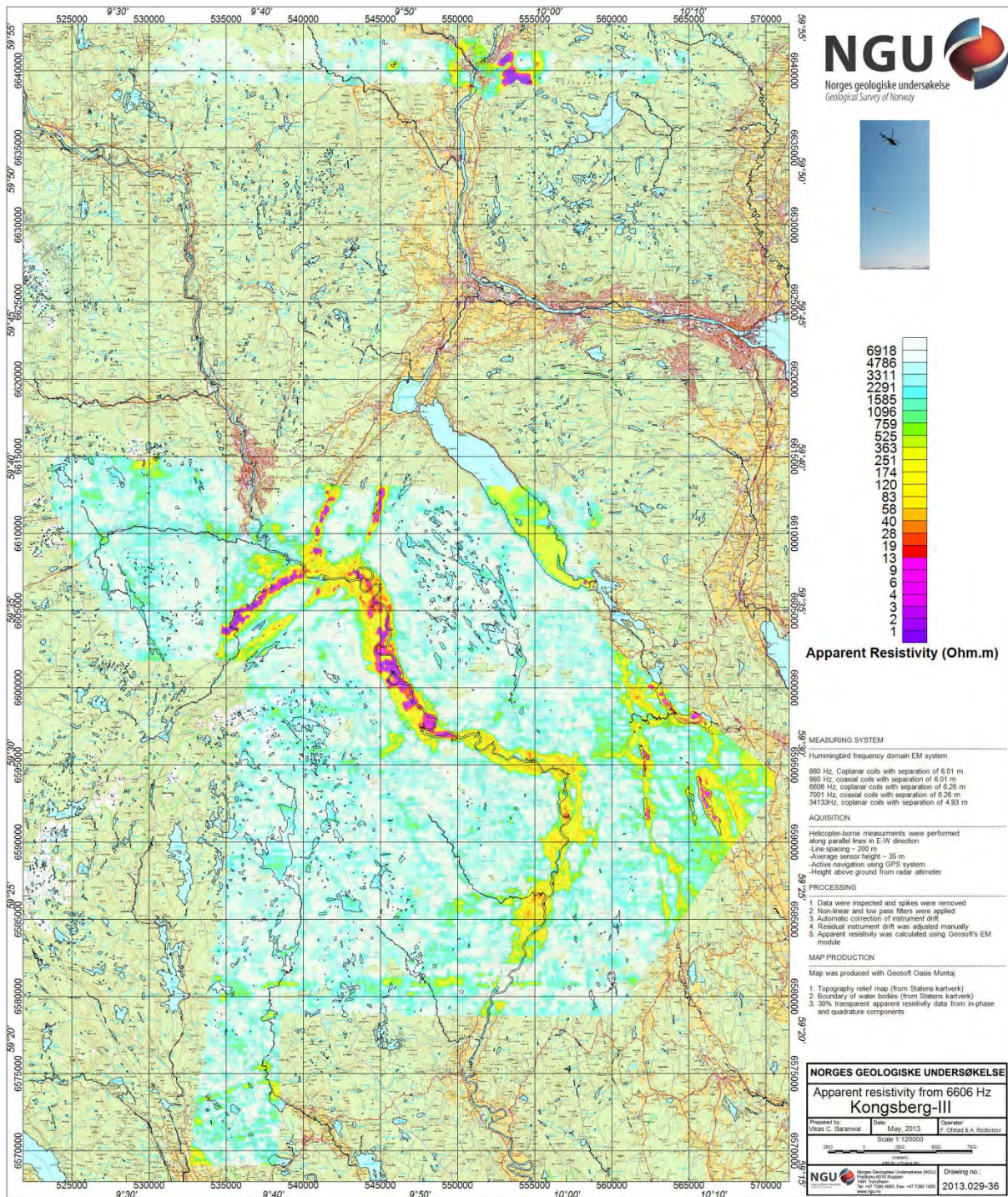


Figure 38: Apparent resistivity map from frequency 6606 Hz from Kongsberg-III.



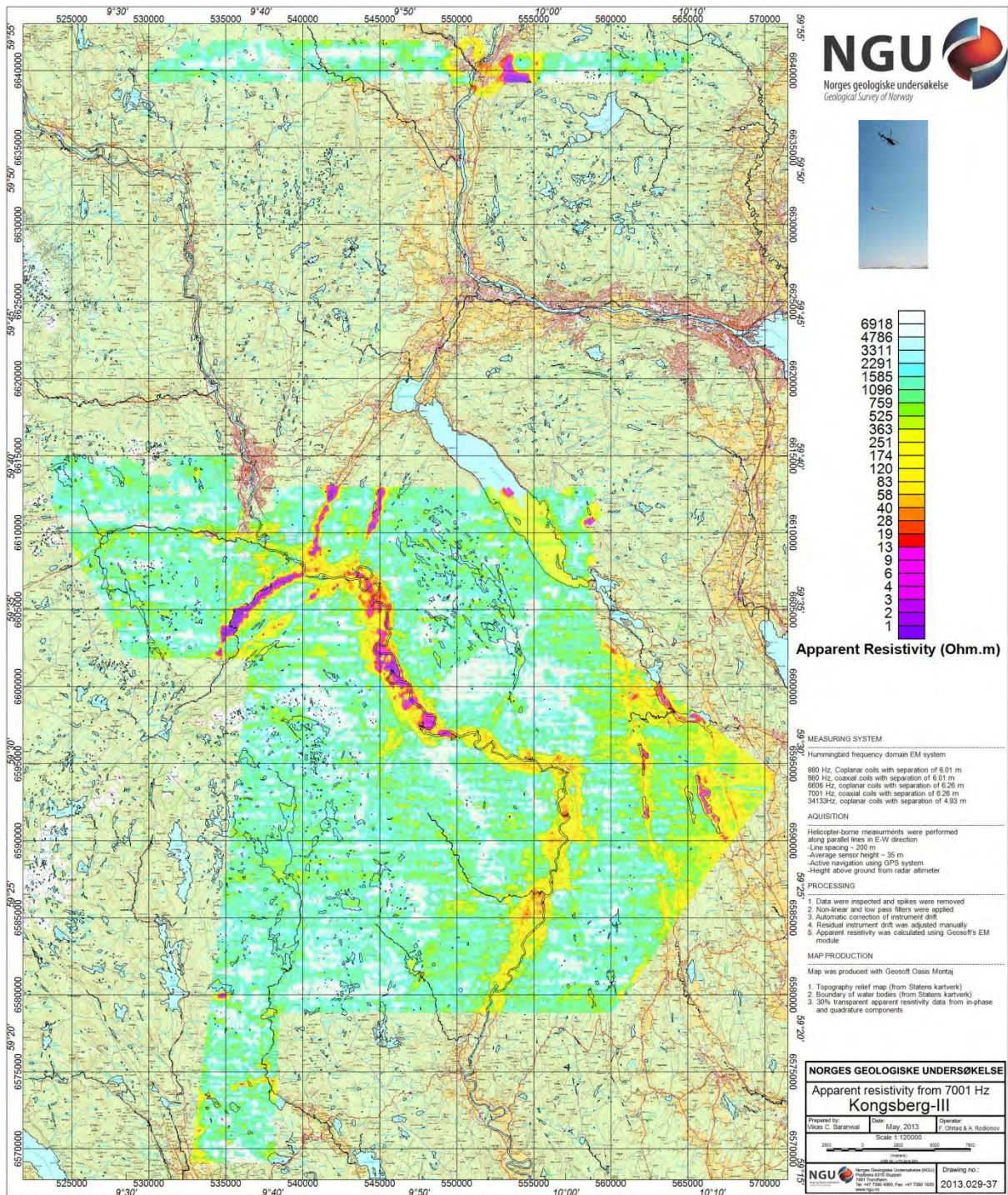


Figure 39: Apparent resistivity map from frequency 7001 Hz from Kongsberg-III.



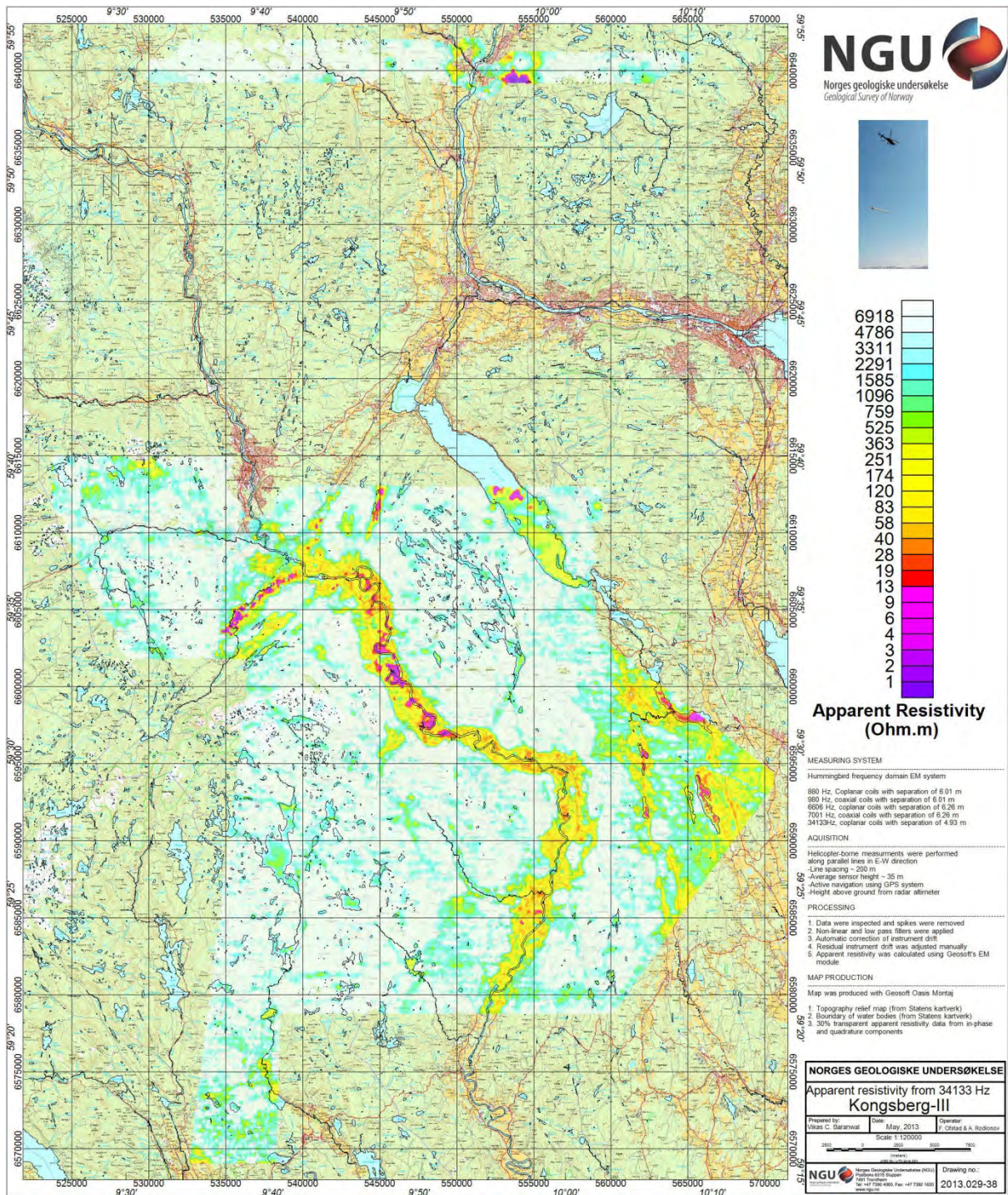


Figure 40: Apparent resistivity map from frequency 34133 Hz from Kongsberg-III.



## **Appendix A: Short description of magnetic, electromagnetic and radiometry methods**

### Magnetic:

Airborne magnetic surveying is an efficient method to determine the main geological, near surface structures and lineaments provided that the associated rock types have measurable magnetic properties<sup>1</sup>. Although a magnetic field is a vector field, essentially all modern instruments in common use measure only the total magnetic field. Local magnetic anomalies related to the magnetization of near-surface rock types are superimposed with the much larger main earth fields (in the order of 50000 nT), other regional anomalies and time-varying external fields (usually in the range of ~ 60 nT). The so-called diurnal magnetic field is mainly caused by the interaction of charged particles emitted from the sun with the geomagnetic field. By using a magnetic base station situated close to the surveyed region, the effect of this slowly varying external field can be measured and removed from the magnetic helicopter data. However, in some periods so-called magnetic storms occur that are responsible for strong high-frequency magnetic noise which is difficult to remove using base station corrections. Magnetic surveying should not be carried out during these periods.

### Electromagnetic:

Airborne EM methods are well-established geophysical methods to determine conductive structures in the subsurface and are very popular in mineral explorations, because many ore deposits, particularly sulfides, are characterized by increased conductivities. Thus, EM systems are capable of directly detecting conductive ore. However, conductivity variations are also present due to the variation in water content of rock, and due to the effects of alteration (silicic alteration would create a resistivity high, whereas sericitic and potassic alteration would create a resistivity low).

Frequency-domain EM systems<sup>2</sup>, of the type used in this survey, consist of one or several sets of transmitter and receiver coils that are fixed<sup>3</sup> directly to so-called bird towed from the helicopter. For frequency-domain systems each transmitter coil generates a sinusoidal electromagnetic field. These primary fields induce currents in conductive underground structures producing time-invariant secondary magnetic fields. In turn these secondary magnetic fields induce a current in the corresponding receiver coils. Because different discrete frequencies and geometric configurations (e.g. horizontal coplanar = both coils are parallel to the horizontal; coaxial = both coils are orientated normal to the flight direction) are sensitive to other conductivities ranges and geometric characteristics of subsurface, helicopter EM frequency systems have several different coil sets. The coaxial sets tend to couple better with vertical structures, while the horizontal coils couple better with flat-lying structures.

---

<sup>1</sup> The local magnetic field of rocks is typically sensitive to the magnetite content. Therefore classification based on magnetic anomalies varies from other geological classification methods which are often silica based.

<sup>2</sup> In addition to frequency domain systems also time-domain systems (TEM) exist for airborne investigations. Such time-domain systems generate short-term pulses and use the decay characteristics of the secondary field to determine conductivity distributions in the ground.

<sup>3</sup> The advantage of fixing the coils is that the transmitted primary field has always constant amplitude at the receiver, and thus can be accurately removed from the secondary fields scattered by the earth. Since the primary field is by definition in-phase, fixing the coils means that the in-phase component of the transmitted field can be accurately removed from the in-phase component of the total field measured at the receiver. This in turn means that the in-phase component of the scattered field from the ground can be accurately determined. This is not the case for systems where the transmitter and receiver geometry is not fixed.

To calculate the apparent conductivities (resistivities) in the ground, amplitudes of the in-phase (real) and/or quadrature (imaginary) part of the secondary signals are used either in a lookup table method or in an iterative inversion procedure. In this survey, the inversion method was used. Thereby, "apparent" means that the used forward model is based on homogenous half-space assumption and only one conductivity value is calculated for each data point. In this context it is important to note that in-phase amplitudes are not only dependent on conductivities (resistivities), but also on magnetic susceptibility in the near-surface ground. Magnetic susceptibility reduces the in-phase amplitudes such that lower apparent resistivities values are obtained from inversion of the in-phase than from inversion of the corresponding quadrature channels in magnetic regions<sup>4</sup>.

During measurements not only the secondary field, but also the primary field is detected from the receiver. This primary field is several decades larger due to the short distance from the transmitter coil and have to be reduced during operation. The NGU system uses so-called "bucking coils" (located close to the transmitter coils) to remove much of the signal from primary field in the receiver coils. However, attenuation of the primary field is not perfect and therefore specific calibrations routines ("nulling" and "phasing") are performed before each field campaign.

Small changes in the transmitter-bucking–receiver coil geometry, as well as changes in the electrical properties of the coils and amplifiers in the receiver-bucking coil circuit introduces a slowly varying background drift signal that overprints the secondary field from the ground. This drift must be removed in processing before the secondary field can be used to compute an apparent resistivity. Removal of such a drift is the by far most time-consuming and challenging part of the processing.

Small signal amplitudes close to the noise level provide less reliable apparent resistivity estimates. Therefore, low amplitude in-phase/quadrature data should be considered carefully. Amplitude level of in-phase/quadrature data are governed by several factors:

- Amplitude level increases with conductivity both for in-phase and quadrature data as long as the conductivities are not particularly high. This means more resistive structures are more difficult to identify from EM data.
- In-phase data can be negative where the ground is resistive and magnetic.
- Horizontal coplanar configuration is more sensitive to horizontal structures and its data have usually larger amplitudes than the ones from the coaxial configuration.
- For structures with conductivities typical for many rock types signals from higher frequencies have larger amplitudes than the ones from lower frequencies.

Basic principles of airborne and helicopter borne EM methods are described by e.g. Palacky and West (1991). One among many other recent reviews about EM methods is presented by Fitterman and Labson (2005).

### Radiometry:

Airborne gamma ray spectrometry (AGRS) is generally used for mapping of the near-surface concentration of the natural isotopes Thorium-232, Uranium-238 and Potassium-40, whose decay series are responsible for mostly all radioactivities from natural sources. <sup>40</sup>K has only one daughter product (<sup>40</sup>Ar), but <sup>238</sup>U and <sup>232</sup>Th decay in a series of 18 and 11 daughter isotopes until the stable isotopes <sup>206</sup>Pb and <sup>208</sup>Pb are reached. AGRS can also be used for environmental surveys e.g. to map Cs fallout from the Chernobyl accident. In case of Cs

---

<sup>4</sup>Only the induced but **not** the remnant magnetization has an effect onto the in-phase amplitude.



mapping, two isotopes of Cs could be present,  $^{134}\text{Cs}$  and  $^{137}\text{Cs}$ ; however  $^{134}\text{Cs}$  has a half-life of only 730 days. All  $^{134}\text{Cs}$  from Chernobyl would have effectively disappeared, and so we map only  $^{137}\text{Cs}$  which has a longer half-life of 11000 days.

Every product in the decay series has its own specific alpha, beta and/or gamma radiation. During measurements the gamma radiation is recorded by a scintillation detector and arranged into a spectrum of 1024 equally sized energy channels. In the processing, it is possible to separate the contribution of the K, U and Th from the total spectra by using the gamma ray counts in windows around the most significant energy maxima of the decay series. For uranium and thorium series the maxima from the daughter products  $^{214}\text{Bi}$  and  $^{208}\text{Tl}$  are used. The counts in these windows represent the Uranium and Thorium ground concentrations assuming that the products in the decay series are in equilibrium (it is assumed that no products are depleted or added)<sup>5</sup>. For determining Potassium ground concentrations, counts in a window around the  $^{40}\text{K}$  peak are used. Cs concentration is determined from counts in a window around the  $^{137}\text{Cs}$  peak.

Any spectrum measured with an airborne system will be a mixture of spectra from various sources including cosmic radiation, aircraft background, atmospheric radon background, naturally occurring  $^{40}\text{K}$ ,  $^{238}\text{U}$ ,  $^{232}\text{Th}$  from ground,  $^{137}\text{Cs}$  from nuclear accidents, and other man-made radioactive nuclides. In natural radioelement surveys, the cosmic, aircraft and atmospheric radon signals are considered as background: for fallout mapping, the gamma rays from natural radioelements in the ground will also be considered as background.

Gamma radiation is strongly attenuated by any type of shielding/covering materials and therefore only the gamma radiation from the upper one meter of the subsurface is recorded by helicopter-borne gamma ray spectrometry. This means that information from gamma ray spectrometry is always limited to the shallow features. Soil and sediments (but also high water concentrations in the shallow ground) can significantly attenuate gamma radiation from underlying rock. However, in region with no or thin overburden, radiometry data can often provide accurate "geological maps", because uranium, thorium and potassium concentrations are closely linked to individual rock types and their origin/development. Because the number of radiation counts from surface material decreases exponentially with the altitude above the ground, data quality of radiometric airborne data is strongly dependent on the flight heights. Weather conditions and air radon concentrations ( $^{222}\text{Rn}$ ) also have a large impact on the data quality and can complicate the data processing. A complete overview (including theory, calibration, acquisition, processing and interpretation) of gamma ray spectrometry methods is given in IAEA (2003).

---

<sup>5</sup> To emphasize that  $^{238}\text{U}$  and  $^{232}\text{Th}$  concentrations are not directly measured, finally determined uranium and thorium concentrations are presented in "eU" and "eTh". The prefix "e" stands for "equivalent" or "effective".

## Appendix B1: Flow chart of magnetic processing

Meaning of parameters is described in the referenced literature.

Processing flow:

- Quality control.
- Visual inspection of airborne data and manual spike removal
- Conversion of ASCII data file from magbase station to Geosoft \*.bas files
- Import magbase data to Geosoft database
- Inspection of magbase data and removal of spikes
- Correction of data for diurnal variation
- Splitting flight data by lines
- Gridding
- Microlevelling if required

## Appendix B2: Flow chart of EM processing

Meaning of parameters is described in the referenced literature.

Processing flow:

- Filtering of in-phase and quadrature channels with non-linear and low pass filters
- Automated leveling
- Quality control
- Visual inspection of data.
- Splitting flight data by lines
- Manual removal of remaining part of instrumental drift
- Calculation of an apparent resistivity for each frequency using both - in-phase and quadrature channels
- Gridding

## Appendix B3: Flow chart of radiometry processing

Underlined processing stages are not only applied to the K, U and Th window, but also to the total counts. Meaning of parameters is described in the referenced literature.

Processing flow:

- Quality control
- Airborne and cosmic correction (IAEA, 2003)  
Used parameters: (determined by high altitude calibration flights near Narvik airport in August, 2011 and from Rønning et al., 2003)

Aircraft background counts:

	Kongsberg-I	Kongsberg-II	Kongeberg-III
K window	10	10	9
U window	3	3	3
Th window	3	3	0
Uup window	0	0	0
Total counts	150	150	150

Cosmic background counts (normalized to unit counts in the cosmic window):

	Kongsberg-I	Kongsberg-II	Kongeberg-III
K window	0.039	0.039	0.0610
U window	0.029	0.029	0.0454
Uup window	0.008	0.008	0.0237
Th window	0.034	0.034	0.0626
Total counts	0.68	0.68	1.0536

- Radon correction using upward detector method (IAEA, 2003)  
Used parameters (determined from survey data over water and land):



Kongsberg-I		Kongsberg-II		Kongeberg-III	
$a_U$ : 0.18	$b_U$ : 1.93	$a_U$ : 0.26, 0.46	$b_U$ : 0.13, -0.44	$a_U$ : 0.18	$b_U$ : 1.93
$a_K$ : 0.94	$b_K$ : 7.73	$a_K$ : 0.80, 0.80	$b_K$ : 3.10, 3.94	$a_K$ : 0.94	$b_K$ : 7.73
$a_T$ : 0.16	$b_T$ : 0.98	$a_T$ : 0.05, 0.10	$b_T$ : 0.50, 1.22	$a_T$ : 0.16	$b_T$ : 0.98
$a_{TC}$ : 16.84	$b_{TC}$ : 22.18	$a_{TC}$ : 12.49, 12.43	$b_{TC}$ : 13.50, 62.03	$a_{TC}$ : 16.84	$b_{TC}$ : 22.18
$a_1$ : 0.100	$a_2$ : -0.02	$a_1$ : 0.066, 0.293	$a_2$ : 0.003, 0.016	$a_1$ : 0.100	$a_2$ : -0.02

- Stripping correction (IAEA, 2003)

Used parameters (determined from measurements on calibrations pads at the NGU):

	Kongsberg-I	Kongsberg-II	Kongeberg-III
a	0.0482	0.0567	0.0482
alpha	0.3087	0.3169	0.3087
beta	0.4807	0.5175	0.4807
gamma	0.7953	0.7377	0.7953

- Height attenuation correction to a height of 60 m from measured and calculated STP height  
Used parameters (determined by height calibration flight at near Narvik airport in August, 2011 and from Rønninget al., 2003):

Attenuation factors in 1/m:

	Kongsberg-I	Kongsberg-II	Kongeberg-III
K:	0.0082	0.0082	0.0107
U:	0.0084	0.0084	0.0067
Th:	0.0066	0.0066	0.0062
TC:	0.0067	0.0067	0.0076

- Converting counts at 60 m heights to element concentration on the ground

Used parameters (determined from NGU calibration pads):

Counts per elements concentrations:

	Kongsberg-I	Kongsberg-II	Kongeberg-III	
K:	80.28	83.8	69.1	counts/%
U:	6.97	7.11	7.71	counts/ppm
Th:	4.28	3.95	4.38	counts/ppm

- Microlevelling if required

## Appendix C: Description of channel labels used in XYZ files

X_ and Y_	: X and Y coordinates in UTM zone 32
UTC_Time	: UTC time
ALT_R_M	: Height (of helicopter) in meters from the ground
ALT_R_M_STP	: Height calculated at STP (of helicopter) in meters from the ground
ALT_R_EM	: Height (of EM bird) in meters from the ground
Mag_Anom	: IGRF corrected Total magnetic field anomaly in nT
R_TC_60m	: Total radiation count calculated at 60 m height in counts/sec
R_K_perc	: Ground concentration of potassium in percentage
R_U_ppm	: Ground concentration of equivalent uranium in parts per million
R_Th_ppm	: Ground concentration of equivalent Thorium in parts per million
..._MICNGU	: Microlevelled data using NGU's in-house software
E_0i_880_F_L	: Levelled(L) in-phase(i) Electromagnetic(E) data in ppm at frequency 880 Hz(880) from coils in horizontal coplanar geometry(0)
E_1q_980_F_L	: Levelled(L) quadrature(q) Electromagnetic(E) data in ppm at frequency 980 Hz(980) from coils in vertical co-axial geometry(1)
..._6k_...	: at frequency 6606 Hz(6k)
..._7k_...	: at frequency 7001 Hz(7k)
..._34k_...	: at frequency 34133 Hz(34k)
E_RES_880_Q	: Apparent resistivity (RES) in ohm.m calculated from quadrature(Q) component at frequency 880 Hz(880)
..._IQ	: calculated from in-phase and quadrature(IQ)
..._neg	: In-phase and quadrature values were multiplied by -1 to correct it for sign conversion to calculate correct apparent resistivity





Norges geologiske undersøkelse  
Postboks 6315, Sluppen  
7491 Trondheim, Norge

Besøksadresse  
Leiv Eirikssons vei 39, 7040 Trondheim

Telefon 73 90 40 00  
Telefax 73 92 16 20  
E-post [ngu@ngu.no](mailto:ngu@ngu.no)  
Nettside [www.ngu.no](http://www.ngu.no)

*Geological Survey of Norway  
PO Box 6315, Sluppen  
7491 Trondheim, Norway*

*Visitor address  
Leiv Eirikssons vei 39, 7040 Trondheim*

*Tel (+ 47) 73 90 40 00  
Fax (+ 47) 73 92 16 20  
E-mail [ngu@ngu.no](mailto:ngu@ngu.no)  
Web [www.ngu.no/en-gb/](http://www.ngu.no/en-gb/)*